Ultrasound Stimulated Acoustic Emission
for Monitoring Thermal Surgery

by

Jonathan S. Thierman
Bachelor of Science, Biomedical Engineering & Engineering Sciences
Harvard University, 1998

Submitted to the Department of Mechanical Engineering in partial fulfillment of the
requirements for the degree of

MASTER OF SCIENCE IN MECHANICAL ENGINEERING

at the

MASSACHUSETTS INSTITUTE OF TECHNOLOGY

FEBRUARY 2001

© 2001 Jonathan S. Thierman. All rights reserved.

Signature of Author.......

Department of Mechanical Engineering
January 19, 2001

Certified by.........................

Kullervo Hynynen, Ph.D.
Associate Professor of Radiology, Harvard Medical School
Thesis Advisor
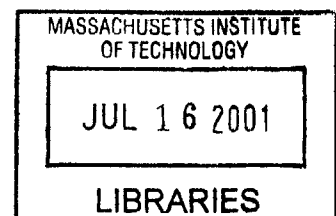
Certified by...........

Ernest G. Cravalho, Ph.D.
Professor of Medical & Mechanical Engineering, M.I.T.
Departmental Advisor

Accepted by...........................

Ain A. Sonin, Ph.D.
Chairman, Committee on Graduate Students
Department of Mechanical Engineering

Ultrasound Stimulated Acoustic Emission for Monitoring Thermal Surgery

by

Jonathan S. Thierman

Submitted to the Department of Mechanical Engineering in partial
fulfillment of the requirements for the degree of Master of Science in
Mechanical Engineering at the Massachusetts Institute of Technology
January 19, 2001.

Abstract

Therapeutic ultrasound describes a non-invasive surgical technique by which high-energy
ultrasound is delivered to malignant tissue. This method must be monitored in order to
ensure that the correct tissues are treated and that the tissues are treated with the proper
dose. Typically, therapeutic ultrasound has relied on MRI techniques to monitor the
extent of the thermal surgery. Besides for the great cost and limited availability, MRI
monitoring presents limitations for therapeutic equipment design because all other
equipment must be compatible with the large magnetic fields created by the MRI system.
A new method of monitoring is explored which uses a method coined Ultrasound
Stimulated Acoustic Emission, USAE. This relatively new material property
measurement method presented by M. Fatemi and J.F. Greenleaf in *Science* May 1998
relies on the low frequency stimulation of a material by overlapping two slightly differing
high frequency ultrasound beams in a pattern which creates a region of low frequency,
known as a beat frequency. The resulting low frequency stimulus is highly focused and
localized. The low frequency pressure field causes cyclic forces and induces a
mechanical displacement in the object being imaged. The low frequency response of the
object from the ultrasound stimulus reveals information about the mechanical and
ultrasound properties of the object, namely its stiffness and acoustical absorption
coefficient. A diagnostic ultrasound system applying the USAE method for imaging
biological tissues was designed and constructed for use in this thesis.

In a series of experiments presented in this thesis, the USAE method is applied to
imaging ex vivo porcine and rabbit tissue. Lesions are created with focused ultrasound
and raster scanned in the focal plane by the two intersecting focused ultrasound fields to
image the necrosed tissue. This method successfully rendered high-resolution images of
the necrosed lesions. In addition, the amplitude of the USAE responses correlate well

with temperature measurements in a study of nine samples of porcine fat and nine samples of porcine muscle. Evidence including a broadband response and fluctuating USAE amplitude indicate that the USAE method may also be used to detect cavitation events in tissue. The images and the temperature measurements demonstrate the effectiveness of the USAE method for imaging and monitoring biological tissue in conjunction with thermal therapy.

Thesis Advisor: Kullervo Hynynen, Ph.D.
Title: Professor of Radiology, Harvard Medical School and Brigham and Women's Hospital

Acknowledgements

LIST OF FIGURES

7

LIST OF TABLES

1 Introduction

Therapeutic ultrasound is proving to be an increasingly effective method for treating various cancers and other non-malignant pathologies in humans. Studies have demonstrated the effective use of phased arrays as non-invasive surgical tools [24]. Traditionally, MRI has been used to monitor the damaged tissue and temperature elevations during such non-invasive procedures. However, problems with MRI monitoring of ultrasound therapy include the high cost and limited availability of MRI systems.

An ideal monitoring system would utilize the same transducer that applied the ultrasound therapy, thereby eliminating extraneous equipment and the large added cost of an MRI system. One solution is to apply the method of vibro-acoustography to image the changing mechanical properties of the sonicated tissue.

Ultrasound stimulated vibro-acoustography (USVA)[1] refers to an imaging method presented by M. Fatemi and J.F. Greenleaf [11] that utilizes the mechanical response of an object to local cyclic radiation forces. These forces result from a complex pressure field produced by an ultrasound transducer. Applying these cyclical forces to an object leads to the mechanical motion of the object. The amplitude of this response from the object is a function of its mechanical and radiation impedances as described by Fatemi and Greenleaf [13]. Therefore, we can determine mechanical properties of an object by observing the amplitude of the response from these cyclical forces. The unique feature of

---

[1] This method is referred to as ultrasound stimulated acoustic emission (USAE) throughout the remainder of this thesis. Both USVA and USAE were coined by Fatemi and Greenleaf [11].

this method is that high spatial resolution can be obtained by applying the cyclical force to only a small point in space by overlapping two tightly focused ultrasound fields of slightly differing frequencies. The resulting "beat frequency" will be the low frequency difference between the two overlapping fields and will only occupy a small volume in space.

We have tested the feasibility of using the USAE signal for controlling thermal surgery. We hypothesize that the USAE signal is temperature-dependent because many tissue properties influencing the radiation force are temperature-dependent. In addition, it is known that the stiffness and absorption coefficient of tissue increases as proteins coagulate [58, 62]. Therefore, the USAE method should also be able to detect coagulated tissue.

The first step in this design of a new ultrasound monitoring system is to determine if USAE can be used to image tissue, and if it can be made sensitive enough to distinguish between the necrosed tissue of a lesion and healthy tissue.

1.1 Focused Ultrasound Surgery

Focused Ultrasound Surgery (FUS) uses highly focused ultrasound radiation to cause thermal changes in the focal volume with little thermal effect on the near field. Ultrasound energy can cause thermal changes by both acoustical absorption and by the implosion of cavitation bubbles induced by high-pressure ultrasound waves. Although the cavitation mode shows potential, [36,44,48,60] the acoustical absorption mode is more easily characterized and yields lesion sizes and shapes which are well predicted by

mathematical models [8,10]. In addition, therapy which utilizes acoustical absorption is easily monitored with thermometry whereas therapy involving cavitation bubbles can cause sudden and drastic temperature fluctuations.

FUS has been developed for use in several applications involving noninvasive tissue treatment including coagulation necrosis [15] and hyperthermia [35]. Researchers have investigated the use of FUS for treatment in several organ systems including breast, liver, prostate, and brain. [2,3,7,14,17,19,34,35,40,43,49,53,54,57].

FUS exploits a narrow band of therapeutic frequencies between .5 to 4 MHz. In this spectral window, the balance between penetration depth and focusing volume size is optimal such that a tight focus (1-5mm diameter) can be obtained with little power deposition in the near field. A typical ultrasound wave at 1.0 MHz has a wavelength of 1.5 mm and a penetration depth of roughly 10 cm in soft tissue [20]. In comparison, a microwave, which radiates at 2450 MHz has a wavelength of 1.8 cm and a penetration depth of only 1.7 cm in tissue [28]. Thus, non-invasive surgery 1-20cm below the tissue surface is possible using FUS with little or no near field heating.

1.2 Current Monitoring Methods

The real time monitoring of the location and extent of tissue damage remains one of the greatest challenges in focused ultrasound treatment. It is imperative to have feedback regarding the extent to which tissues have been damaged by focused ultrasound therapy because the intensity and duration of the treatments vary considerably between individuals and between tissue types in the same individual. Biological factors such as

adipose fat thickness, muscular density, and blood perfusion rates can cause variations in the treatment parameters necessary to produce necrosis in the target tissue volume. Many studies have documented these variations [1] and countless articles have been published in an effort to address the need for an effective monitoring system during FUS treatment. Studies of various imaging techniques including diagnostic ultrasound [59], CT imaging [27], and MRI [25] reveal varying degrees of success at monitoring FUS.

1.2.1 Diagnostic Ultrasound

Diagnostic Ultrasound has been investigated extensively as a method for monitoring FUS because it is relatively inexpensive and because it is easily applied due to the fact that FUS already uses an ultrasound transducer. While other imaging modalities require large, specialty equipment, an ultrasound imaging method could be applied with very little alteration to the surgical set-up. Although diagnostic ultrasound utilizes a higher frequency range (3-10 MHz) than therapeutic ultrasound (.5-4 MHz), it is possible to make a combined array with diagnostic and therapeutic elements. Investigators have shown an increase in ultrasonic backscatter [4] [55] and attenuation [4] [4,46] with coagulation. These changes in the ultrasonic properties of the tissue could theoretically be monitored using an ultrasound diagnostic system. However, this imaging method suffers from poor signal-to-noise ratio images. This is still an active field of investigation, but so far, these changes in tissue properties appear too subtle for their detection via an ultrasound diagnostic system, and the results have not been robust enough to suggest their applicability in a clinical setting.

1.2.2 CT Imaging

CT imaging is a radiographic technique utilizing computed tomographic methods to extract 3D information from a series of volumetric projections. Therefore, it images tissue densities (more specifically, the extent of tissue absorption and scattering of electromagnetic radiation in the "x-ray" frequency range). The advantage of this method is its very high spatial resolution (on the order of 1 mm). However, aside from the cumbersome and expensive nature of this imaging method, the image orientation is not convenient for use with FUS surgery. In addition, CT imaging exposes the patient to ionizing radiation and its use is not ideal for monitoring any procedure over an extended period of time.

1.2.3 MRI

MRI utilizes subtle changes in the proton spin relaxation time constant to distinguish between different tissue types. It offers high spatial resolution and can be used to monitor temperatures in tissues [26] as well as tissue changes due to coagulative necrosis. Its effectiveness in monitoring the location and extent of thermal surgery renders MRI the current gold standard in monitoring FUS. MRI has been refined to clinical application by the work of several investigators [23,37]. However, problems with MRI monitoring of ultrasound therapy include the extremely high cost and limited availability of MRI systems. A typical system costs $1-2 million to install and $1500/hour to operate. The high cost makes the use of this system prohibitively expensive for monitoring outpatient procedures and altogether precludes access to these machines by smaller hospitals.

1.2.4 Sonoelasticity Imaging and Elastography

In the last decade, the advent of sonoelasticity imaging [42] and elastography [41] has offered an estimation of the mechanical properties of tissues by measuring the displacement of the tissue (using diagnostic ultrasound) due to a mechanical force. Elasticity imaging techniques may be more reliable than diagnostic ultrasound in the detection and characterization of ultrasound lesions because the mechanical contrast of FUS lesions was found to be up to one order of magnitude [50] as opposed to their small and less reproducible acoustic contrast. The main application of elastography has been the differentiation of benign from malignant tissues in vitro and in vivo [5] [18] [31] given that the difference in their elastic moduli can be up to two orders of magnitude [33]. Elastography has also been applied in the detection and monitoring of laser and ultrasound lesions [51] [29] [47] [9] [50] due to the fact that tissue coagulation has been associated with a change in tissue stiffness [58] [6] [62]. Imaging shear stiffness [38] and detecting FUS lesions [62] may also be possible with new Magnetic Resonance Elastography (MRE) techniques.

Disadvantages associated with sonoelasticity imaging techniques include the fact that they require the use of an additional imaging system together with the FUS treatment and they rely upon an externally applied mechanical stimulus. For some situations where the tissue is externally accessible, such as breast and prostate, this does not pose a significant problem. However, in the case of internal organs, such as the brain and the liver, the application of these techniques is largely unsuccessful. In addition, synchronization with the therapy applicator is often difficult and the application of the external stimulus can cause too much motion of the target such that the reference is lost.

15

1.3 USAE for Monitoring Thermal Surgery

Remote application of the mechanical stimulus in sonoelastic imaging techniques capitalizes on the mechanical contrast between necrosed and healthy tissue while avoiding the complications of externally exciting the target [52] [11] [39] [61]. A recent proposal involves the use of the USAE method in conjunction with FUS ablation for both monitoring and generating tissue damage [30]. This method provides an additional advantage over other remote excitation methods by using a single system for both detecting and creating tissue ablation.

The USAE method may prove a successful technique for monitoring thermal surgery because in theory, the USAE signal is sensitive to changes in the mechanical and acoustical properties of tissue including stiffness, ultrasound absorption coefficient, and temperature. Each of these properties changes during thermal surgery and may be monitored to assess the level of tissue damage incurred during the sonication of a therapeutic array.

The USAE system would utilize the same transducer to send diagnostic USAE pulses as is currently used to apply HIFU[2] surgery. The USAE system could send its short (50 msec) diagnostic pulse at regular intervals during the HIFU procedure to offer a real time measurement of tissue temperature or the degree of tissue necrosis. Surgery with the same transducer could proceed unaffected by these very short pauses in the sonication. It may even be possible to sonicate at two separate but similar frequencies

---

[2] HIFU stands for "High Intensity Focused Ultrasound"

such that the USAE measurements and the sonication occur simultaneously. This method of applying USAE concurrently with therapeutic ultrasound may be even more effective than sending diagnostic pulses during short pauses in the therapy. Moreover, the large amplitudes of the therapeutic sonication would likely provide an excellent signal to noise ratio for the diagnostic measurements.

The USAE method would offer several advantages over the current techniques used to monitor thermal surgery because of the integration of the diagnostic device into the same transducer used to apply the HIFU surgery. The USAE method would be far less expensive than MRI or CT. This savings in cost and equipment needed to monitor HIFU surgery renders HIFU surgery using the USAE method more practical and more readily available. Another advantages of the USAE method is that the imaging and therapeutic device reside in the same location in the same frame of reference. This makes the USAE method more accurate than CT or diagnostic ultrasound in locating the position of necrosed and non-necrosed tissue. Further, the USAE method has the potential to monitor properties other than those which current methods detect. The USAE method may provide mechanical tissue stiffness information not directly available with other monitoring methods like MRI, CT, or diagnostic ultrasound.

The USAE method combined with a therapeutic transducer could offer a self-contained, seamless system that applies high intensity therapeutic ultrasound with real-time, on-line feedback built into the same device. This opens a world of possibilities for control strategies to accurately sonicate diseased tissue while leaving healthy tissue intact.

2 Theory of USAE Method

The USAE method relies on the confluence of two different ultrasound frequency fields. At their intersection, the waves combine additively to form a high frequency waveform which is modulated at a low frequency. The low frequency of the modulation is the difference between the two high frequencies of the original signals. This low frequency (or "beat frequency") drives the sample at a lower frequency than that with which it is sonicated. The beat frequency allows for accurate detection of the sample's response to low frequency at a specific point in the sample. While the beat frequency exists everywhere in the field, it is highly focused at the focal point of the high frequency fields. In this way, a low frequency signal is applied to the sample with the focal resolution of the much higher frequency field. The sample responds to the radiation force produced by the acoustical field and emits a response signal which a hydrophone records. The mathematics of the resulting beat frequency can be derived from fundamental acoustics and is described in a recent paper [32].
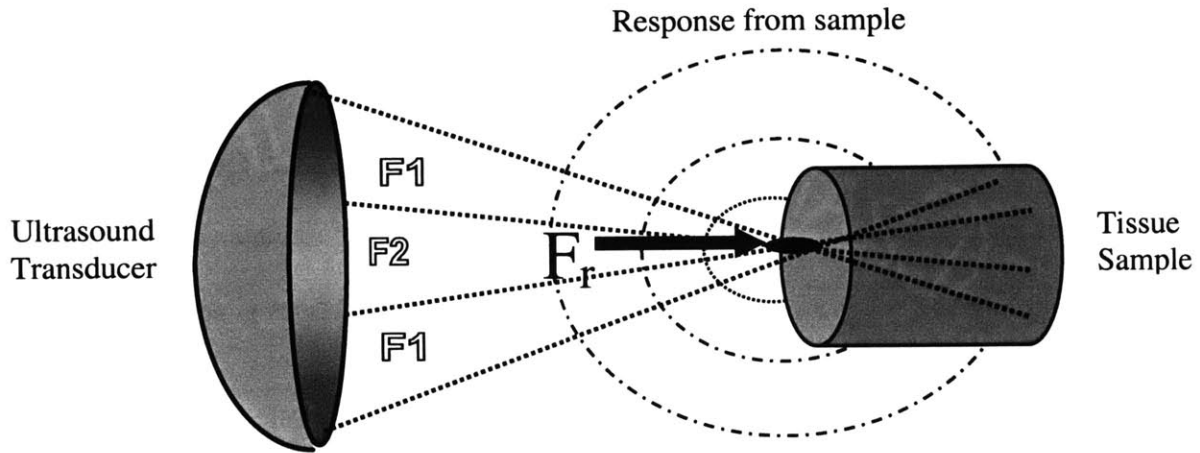
Figure 2-1. Schematic of dual frequency transducer and the radiation force it applies to a sample.

2.1   The Stimulus

The two high frequency beams produced by the dual element transducer can be given by [11],

$$g_1(f_1) = a_1 \cos(2\pi f_1 t + \phi_1) \tag{1}$$

and

$$g_2(f_2) = a_2 \cos(2\pi f_2 t + \phi_2), \tag{2}$$

where $g_1(f_1)$ and $g_2(f_2)$ are the waveforms emitted by the two transducer elements at frequencies f_1 and f_2 with amplitudes a_1 and a_2 and phases ϕ_1 and ϕ_2, respectively. We are interested in the radiation force applied to the sample as a result of these two incident ultrasound waves. This radiation force will drive the sample and elicit the response detected by the hydrophone. The resulting radiation force F applied to the tissue is given by [56],

$$F = \frac{2\alpha I}{c} \tag{3}$$

where α is the absorption coefficient of the tissue sonicated, c is the speed of sound in the tissue and I is the average intensity of the incident beam. F is the short term average radiation force. We use this form to help simplify the integration of the energy term below. The average intensity is related to the average energy by,

$$I = \frac{1}{S}\frac{d\langle E \rangle}{dt} \tag{4}$$

where S is the cross-sectional area of the beam (or intersection area of the two beams, Figure 2-1).

The radiation force is now expressed in terms of the average energy. The average energy can be found by substituting in the original high frequency waves thereby solving for the radiation force in terms of the original high frequency waves. The average energy locally deposited on the object at the focus is given by,

$$\langle E \rangle = \langle (g_1(f_1) + g_2(f_2))^2 \rangle$$

$$= \langle (a_1 \cos(2\pi f_1 t + \phi_1) + a_2 \cos(2\pi f_2 t + \phi_2))^2 \rangle$$

$$= \left\langle 4a_1^2 a_2^2 \cos^2\left(\frac{2\pi(f_1 + f_2)t + \phi_1 + \phi_2}{2}\right)\cos^2\left(\frac{2\pi(f_1 - f_2)t + \phi_1 - \phi_2}{2}\right)\right\rangle$$

$$= \left\langle 2a_1^2 a_2^2 (1 + \cos(2\pi(f_1 + f_2)t + \phi_1 + \phi_2))(1 + \cos(2\pi(f_1 - f_2)t + \phi_1 - \phi_2))\right\rangle$$

$$= \langle A \rangle + \langle cos(2\pi(f_1 + f_2)t + \phi_1 + \phi_2) \rangle + \langle cos(2\pi(f_1 - f_2)t + \phi_1 - \phi_2) \rangle + \langle B \rangle \tag{5}$$

where $\langle \ \rangle$ denotes the short-term time average and A and B substituted above for clarity

are given by,

$$\langle A \rangle = A = 2a_1^2 a_2^2 \qquad (6)$$

and

$$\langle B \rangle = \langle \cos(2\pi(f_1 + f_2)t + \phi_1 + \phi_2)\cos(2\pi(f_1 - f_2)t + \phi_1 - \phi_2) \rangle$$

$$= \int_{-T/2}^{T/2} \cos(2\pi(f_1 + f_2)(t - \tau) + \phi_1 + \phi_2)\cos(2\pi(f_1 - f_2)(t - \tau) + \phi_1 - \phi_2)d\tau$$

$$= \int_{-T/2}^{T/2} \cos(4\pi f_1(t - \tau) + 2\phi_1) - \cos(4\pi f_2(t - \tau) + 2\phi_2)d\tau, \qquad (7)$$

where τ is the integral time variable and T is the period of averaging the energy

deposited.

Given that in the case of vibro-acoustography, $f_1 - f_2 \ll f_1$ or f_2, we choose a

period such that $f_1 - f_2 \ll \dfrac{1}{T} \ll f_1, f_2$ [12]. The result is that $\langle B \rangle$ (Eq. 7) and the

second term of Eq. (5) equal zero. Eq. (5) then becomes

$$\langle E \rangle = AT + A \int_{-T/2}^{T/2} \cos(2\pi(f_1 - f_2)(t - \tau) + \phi_1 - \phi_2)d\tau \qquad (8)$$

$$= AT + \frac{A}{2\pi(f_1 - f_2)}\left[\sin\left(2\pi(f_1 - f_2)\left(\frac{T}{2} - t\right) + \phi_1 - \phi_2 \right) + \sin\left(2\pi(f_1 - f_2)\left(\frac{T}{2} + t\right) + \phi_2 - \phi_1 \right) \right]$$

21

$$= AT + \frac{A}{\pi(f_1 - f_2)} sin(\pi(f_1 - f_2)T) cos(2\pi(f_1 - f_2)t + \phi_2 - \phi_1)$$

We can write this in a more simplified form,

$$\langle E \rangle = C + A_1 [cos(2\pi(f_1 - f_2)t + \phi_2 - \phi_1)] \tag{9}$$

where $C = AT$ and $A_1 = \frac{A}{\pi(f_1 - f_2)} sin(\pi(f_1 - f_2)T)$.

Equation (9) clearly shows that the average energy deposited follows a sinusoidal variation with a frequency equal to the difference frequency of the two resonating transducer elements. A similar result has been reported by Fatemi and Greenleaf [11].

Substituting this average energy term back into Eq. (3) and Eq. (4), while assuming that the two beams encounter the target in phase (i.e., $\phi_1 = \phi_2$), gives the cyclical radiation force resulting from two high frequency ultrasound fields,

$$F = F_0 sin(2\pi(f_2 - f_1)t) \tag{10}$$

where

$$F_0 = \frac{4\alpha A}{cS} \tag{11}$$

Equations (10) and (11) are essential in this research. They show that applying two beams with an intersection cross-sectional area S will locally force the tissue to vibrate in a sinusoidal manner at a frequency equal to the difference between the

frequencies of the incident beams (Figure 2-1). The amplitude of the resulting radiation force depends on both the amplitudes of the two beams and the absorption coefficient of the tissue. This is particularly important in the area of ultrasound ablation, where the absorption coefficient is known to increase with temperature and coagulation [16] [21] [4].

It is important to note that the radiation force resulting from the two ultrasound fields is cyclical with a frequency equal to the difference between the frequencies of the two fields. However, the acoustic field consists only of the two high frequency waves. The cyclical radiation force excites the sample at the difference frequency, despite the fact that the acoustical field is comprised only of the higher ultrasound frequencies. This is because the radiation force is derived from the *energy* of the field and not the amplitude. The energy is proportional to the amplitude of the acoustic field squared. Even though the beat frequency contributes no frequency content to the acoustical field (because it is equally negative and positive at the same instances in time), it affects the energy of the field in a sinusoidal manner. When squared, the envelope of the 'beat' frequency modulation is transformed into a sinusoidal term. This term is the cyclically varying energy of the system and contributes to the cyclically varying radiation force produced by the two ultrasound waves.

This can be illustrated best by an example. Suppose we apply two sinusoidal waves g_1 and g_2 which are in phase (set $\phi_1 = \phi_2 = 0$) with frequencies $f_1 = 100$ Hz, $f_2 = 110$ Hz and amplitudes $a_1 = 1$, $a_2 = 1.3$.

$$g_1(f_1) = a_1 \cos(2\pi f_1 t) \qquad \text{and} \qquad g_2(f_2) = a_2 \cos(2\pi f_2 t) \qquad (12)$$

23

The resulting plots of the signal in the time domain and the FFT of the signal in the frequency domain are depicted below.
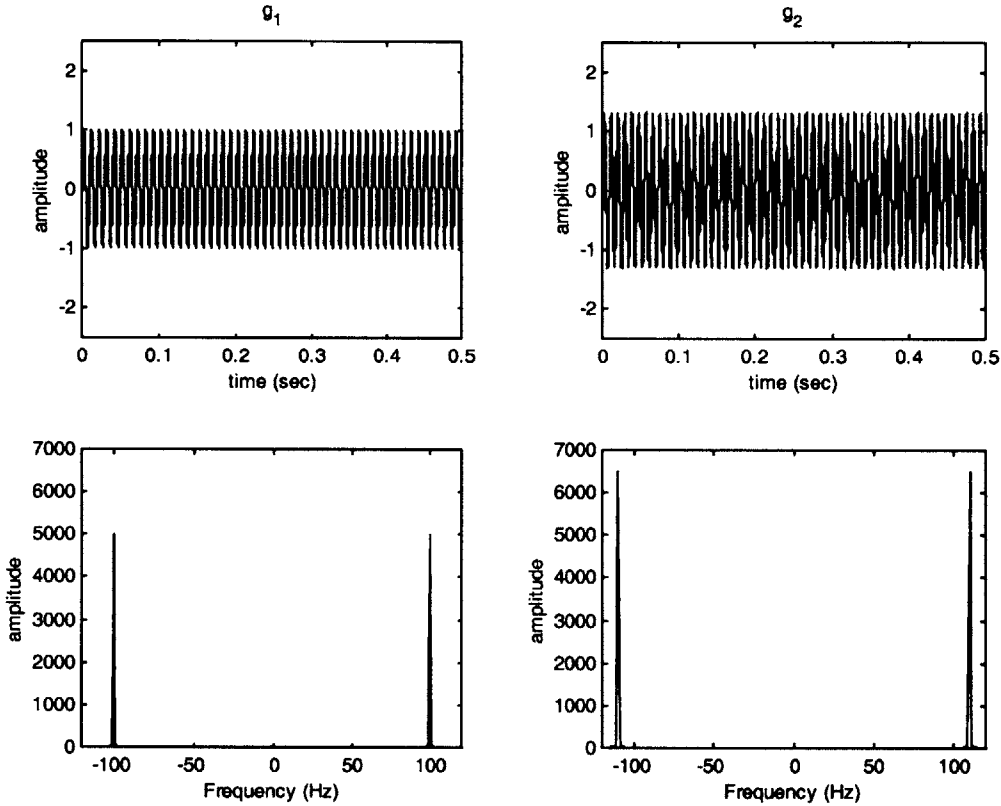
Figure 2-2. Plots of signal g_1 (left column) and g_2 (right column) in time domain (upper plots) and frequency domain (lower plots).

Now, let g_3 be the sum of these two sinusoids in the acoustic field.

$$g_3 = a_1 \cos(2\pi f_1 t) + a_2 \cos(2\pi f_2 t) \qquad (13)$$

with the following time domain and frequency domain plots:
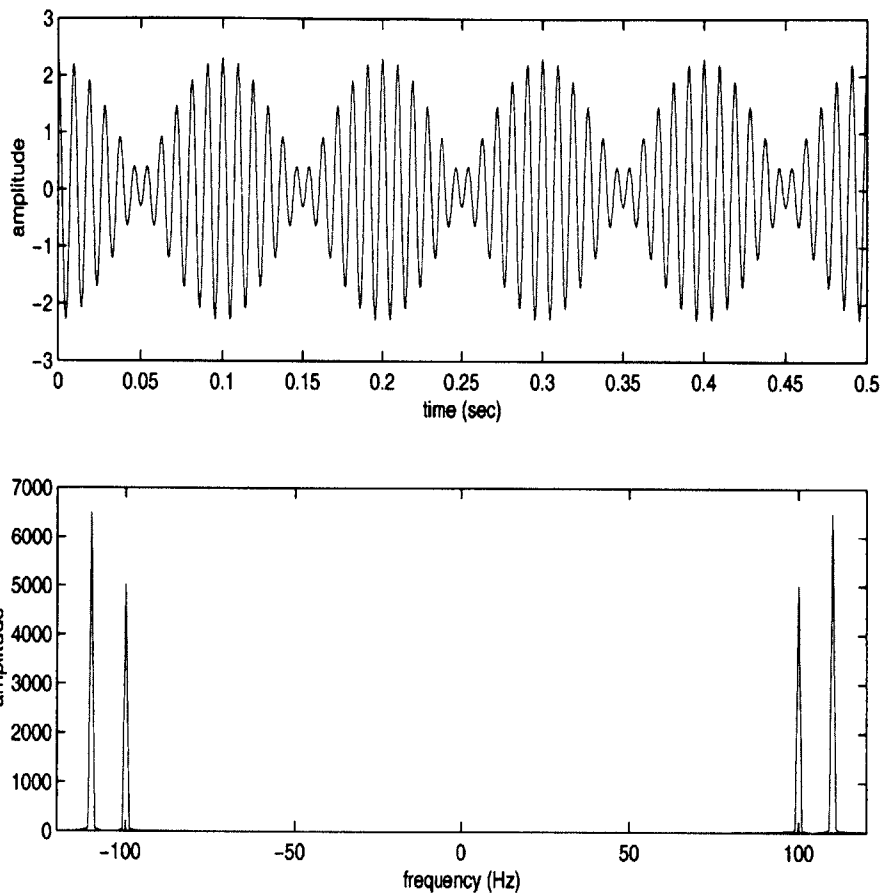
Figure 2-3. Combined signals g_1 and g_2 plotted in time domain (upper plot) and frequency domain (lower plot).

Note the low frequency 'beat' signal formed when the two high frequencies are added. This 'beat' is not a sinusoid but rather a double sided sinusoid because it oscillates in both the positive and negative directions at the same time. In essence, it adds nothing to the frequency content of the signal as observed in the FFT of g_3 above. Instead, the FFT shows only the frequencies of the two high frequency waves which combine to form g_3. However, if we look at the energy content of the acoustic fields

from g_1, g_2, and g_3 we see that the 'beat' frequency of g_3 contributes to a cyclical energy of the field formed from adding g_1 and g_2. The result is a low frequency contribution to the energy produced in the acoustic field by g_3 that is not present in either the fields of g_1 or g_2.
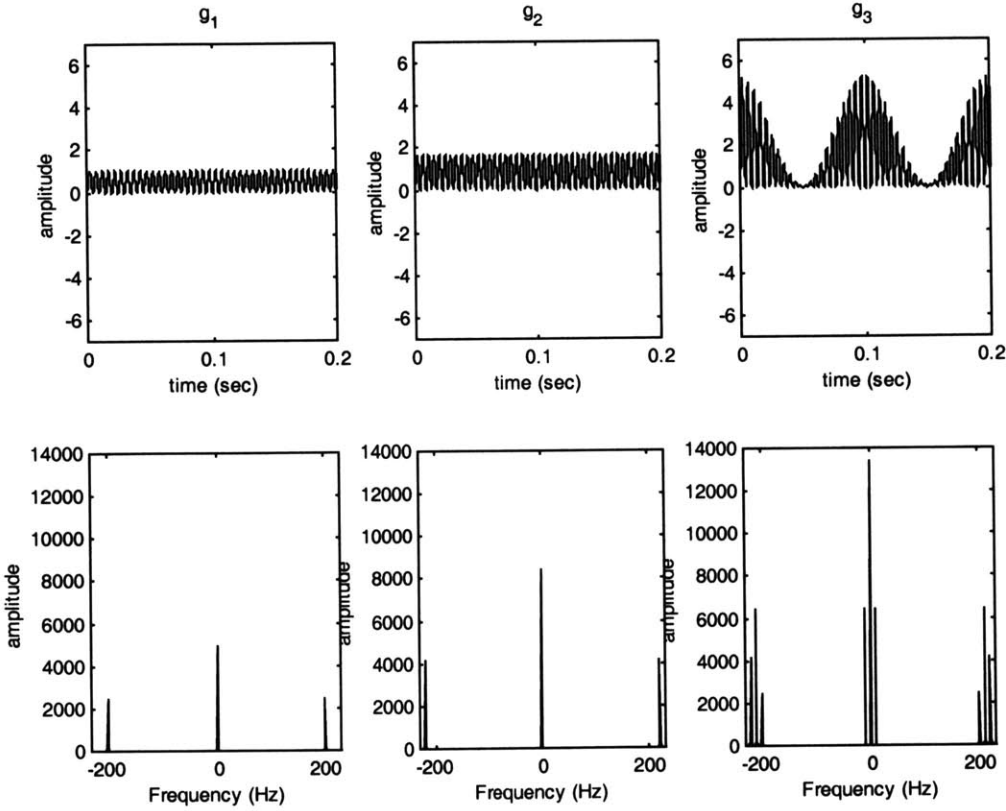
Figure 2-4. Plots of energy for g_1 (column 1), g_2 (column 2), and $g_3 = g_1 + g_2$ (column 3) in time domain (upper plots) and frequency domain (lower plots).

2.2 The Response

The harmonic radiation force results in the harmonic displacement of the tissue, which can be found through the solution of the following simplified equilibrium equation of a linear time-invariant harmonic system [45]:

$$[m]\{\ddot{x}\} + [d]\{\dot{x}\} + [k]\{x\} = F,$$ (14)

where m, d, and k are the mass, damping, and stiffness matrices of the system. F is the applied force given by $F = F_o \cos(2\pi f_0 t)$ where $f_0 = f_2 - f_1$ is the frequency of the radiation force in our case. The displacement, x, is determined by the steady-state solution of Eq. (14)

$$x = X_o \cos(2\pi f_0 t),$$ (15)

where X_o is the amplitude of vibration equal to

$$X_o = \frac{1}{k - m(2\pi f_0)^2} F_o.$$ (16).

Resonance occurs when the excitation frequency f_o equals the resonance frequency of the tissue f_R given by

$$f_R = \frac{1}{2\pi} \sqrt{\frac{k}{m}}$$ (17)

such that X_o goes to infinity.

From equations (11), (15), (16) and (17) it can be concluded that the amplitude of

the sinusoidal displacement resulting from the application of the radiation force depends

on both the stiffness and absorption of the tissue, with the two variables having

counteractive effects. While absorption changes cause a linear change in displacement

amplitude (Eqs. 11 and 16), stiffness changes causes a non-linear, frequency-dependent

effect (Eq. 16). In addition, these equations reveal that the resonance frequency depends

solely on the stiffness of the tissue and not on the absorption (Eq. 17). A resonance

frequency shift will, therefore, occur, if the stiffness of the material changes [12].

The amplitude of the sample response to the dual frequency signal is the main

parameter measured with the USAE method because it depends on the mechanical and

acoustic properties of the sample. This amplitude is recorded with the hydrophone and

calculated using the Fast Fourier Transform X(k) given by,

$$X(k) = \sum_{j=1}^{N} x(j)\omega_N^{(i-1)(k-1)}$$

(18)

where $\omega_N = e^{(-2\pi i)/N}$.

The mechanical model of the response of the sample to the radiation force is a

simplification of the actual problem. It is presented here as an illustration of the effects

of absorption and stiffness in the simplest model of vibration involving a single uniform

object oscillating in 1D. In the actual experiments involving tissue, the sample has six

degrees of freedom. In addition, the tissue has at least two distinct regions of stiffness

due to the necrosed lesion and the non-necrosed tissue regions. To our knowledge, no

analytic solution exists for the problem of displacing a point in an inhomogeneous medium with six DOF. In section 2.3, we use finite-element analysis to study this problem in an attempt to predict the experimental results. The stiffness and absorption properties of tissue change with temperature as well as with necrosis and cavitation. Experiments in calf liver by Wu et al yield the following stiffness and absorption dependences on temperature [62]. These results were also verified with Van Kleef's report on a protein gel [58].
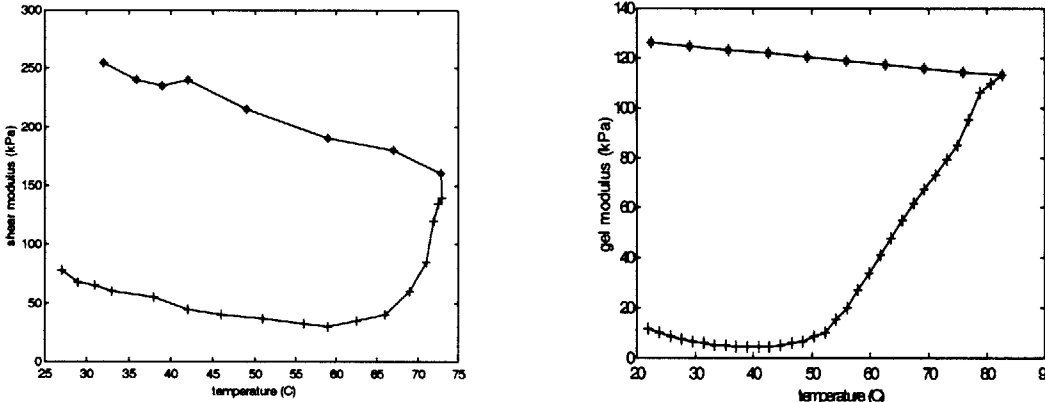
Figure 2-5. Modulus for bovine tissue and a gel phantom during heating and cooling. Data is from experimental results by Wu and by Van Kleef.
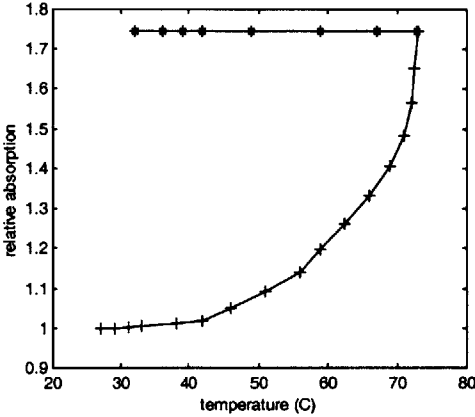
Figure 2-6. Absorption coefficient for bovine tissue during heating and cooling. Data is from experimental results by Wu.

29

2.3 Finite-Element Simulations

In a recent paper, the tissue response to a USAE excitation was modeled on ALGOR[3] by a triangular 2D finite-element grid of size 40x40mm^2 containing an ellipsoidal lesion of a certain size and stiffness [32] with a fixed boundary condition for the entire tissue sample volume. The grid size was chosen to fit the liver tissue samples used in the *in vitro* study of the use of the USAE method for detecting tissue ablation [30]. However, grids of twice that size were also investigated and the overall behavior of the results were similar in both cases. The total number of nodes and elements used was 244 and 426, respectively, with an average distance between adjacent nodes of 1.2 mm. In all cases investigated, the lesion was embedded in a homogeneous background of fixed stiffness (Young's modulus) equal to 12 kPa, which is within the typical modulus range for healthy soft tissues [33]. To simulate soft tissue, the Poisson's ratio was equal to 0.499 and the density was 1000 kg/m^3. The model was axisymmetric so as to take advantage of the inherent symmetry of the problem, i.e., the beam is assumed to excite the tissue on its symmetry axis in the middle of the lesion. The harmonic excitation was applied in the axial direction for 10 ms in order to simulate typical experimental parameters [30]. The displacement was calculated at the same node as the stimulus by solving the differential equation given by Equation 14. No damping is considered to simplify the problem (i.e., the damping matrix in Equation 14 is zero). The sampling rate of the response waveform was 250 kHz with the highest response frequency investigated

---

[3] Algor is a trademark of Algor, Inc., Pittsburg, PA.

equal to 50 kHz. The spectral resolution was 20 Hz for frequencies lower than 1 kHz and 50 Hz for frequencies higher than 1 kHz. The power spectrum of the response waveform was calculated in order to measure the amplitude of the response at the frequency used to excited the node. The maximum amplitude of the power spectrum is the parameter estimated in all subsequent results. All plots display the amplitude of the resulting displacement normalized by the applied displacement.

The effects of lesion absorption and stiffness as well as the frequency range where the USAE method performed optimally were studied with the finite element model. The following three plots show the effect of stiffness (Figure 2-7), absorption (Figure 2-8), and the combination of stiffness with absorption (Figure 2-9) on the response from the finite element tissue model. The ablated tissue stiffness was varied in the model from 1 to 10 times higher than the stiffness of non-ablated (or normal) tissue, covering the range observed experimentally by other authors at both low and high temperatures [50] [62]. The increased absorption coefficient used in the model for ablated tissues was 3 times the healthy tissue level as supported by published experimental results [4]. Note that the frequency spectrum in Figure 2-7 changes in shape as the stiffness is varied and the peak frequencies of the response shift. In Figure 2-8, observe that if the stiffness ratio is held constant, the amplitude at all frequencies of the response increases after ablation due to the frequency-independent increase of the absorption coefficient. Finally, the combined effects of varying the stiffness and the absorption coefficient are modeled. This model reveals that at a given frequency, the result of increasing both absorption and stiffness is not easily predicted. In fact, the two factors work against one another such that the

precise degree to which they increase after ablation will affect the net increase or decrease in the response from the model.
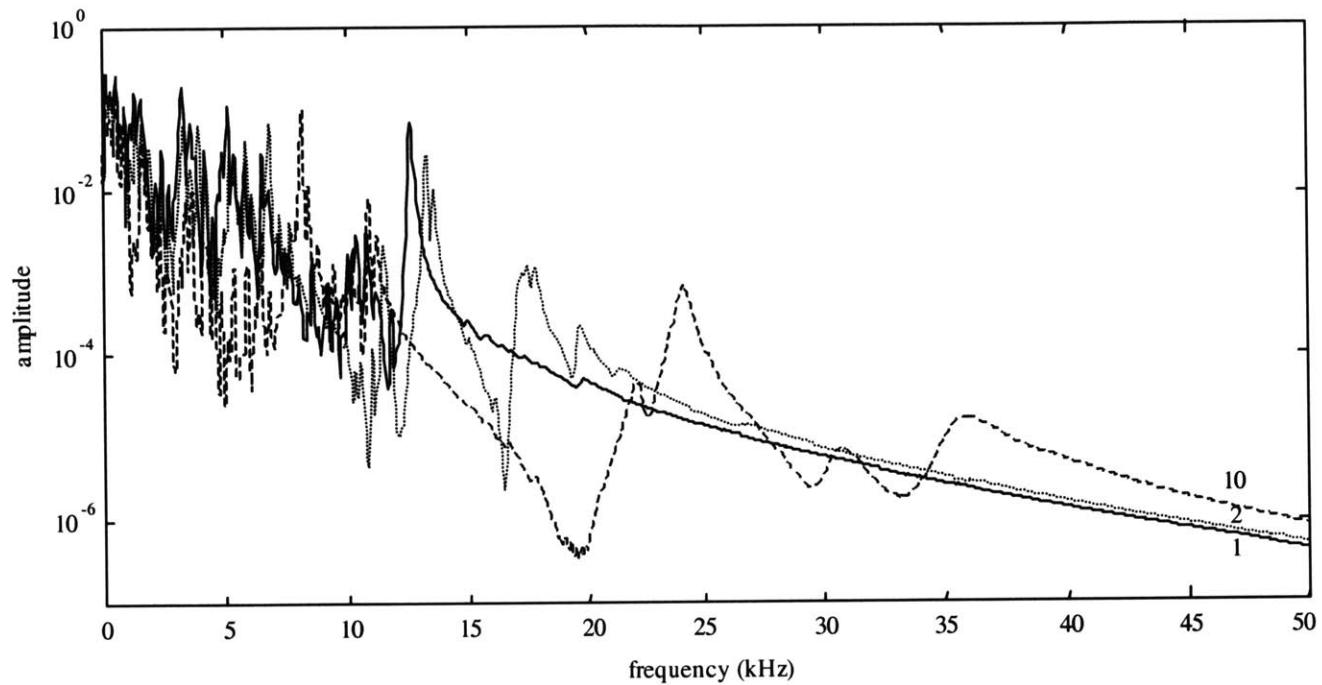
Figure 2-7. Low frequency spectrum at stiffness ratios of one (solid line), two (-.-) and ten (...) . Note that beyond a value of 14 kHz in this example, few resonant peaks occur and kHz the response increases with stiffness above 22 kHz.
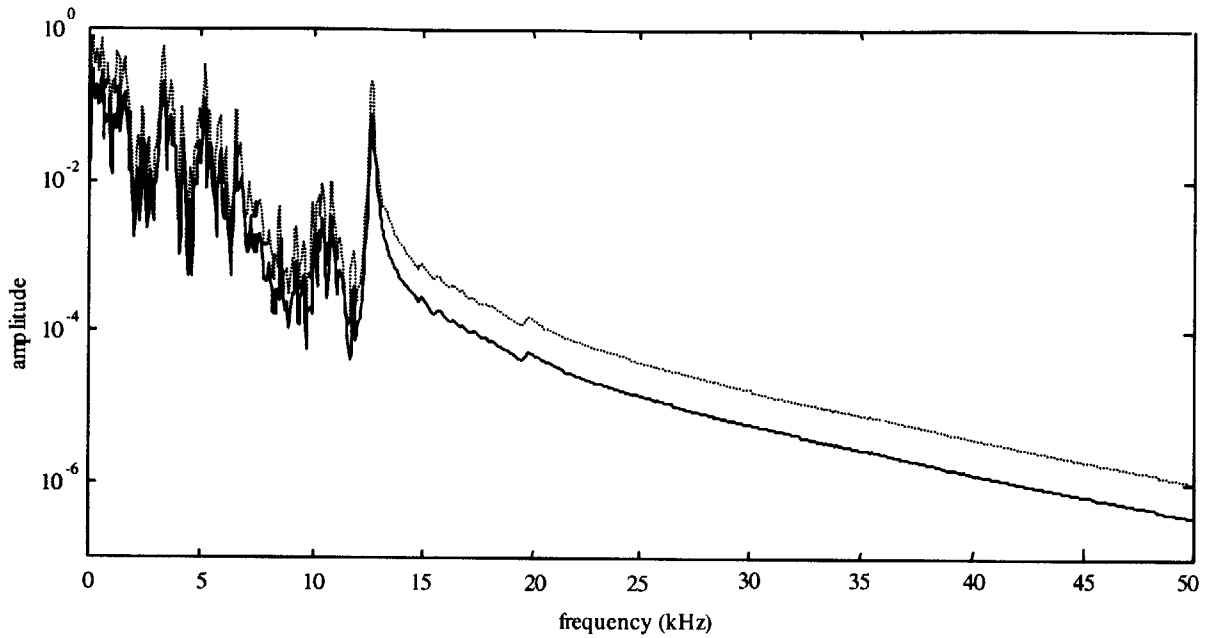
Figure 2-8. Effect of increased absorption coefficient from before (solid) ablation to after (dotted) ablation (lesion-to-background absorption ratio = 3:1, lesion-to-background stiffness ratio of 1:1).
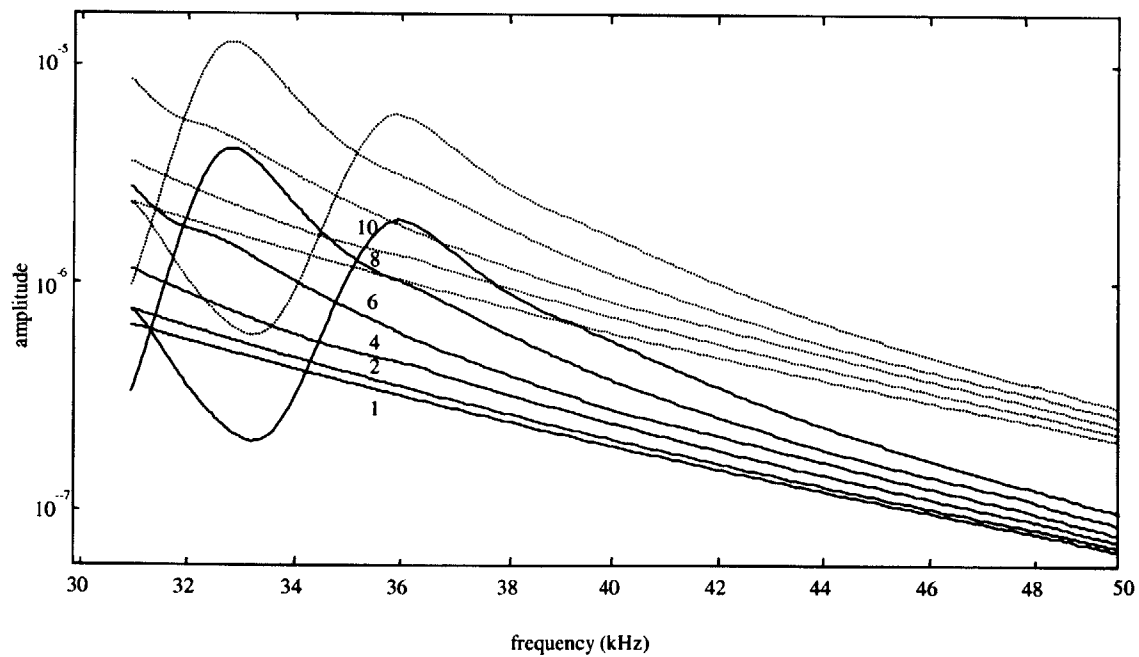
Figure 2-9. High frequency spectrum with (dotted) and without (solid) a 3:1 absorption increase at various stiffness ratios.

3 Experimental Materials and Methods

Experiments were conducted to ascertain the effectiveness with which the USAE method measures changes from healthy to necrosed tissue. There were two different categories of experiments. In one set of experiments, a single optimal difference frequency was determined and then used to sonicate the tissue before and after a lesion of coagulated necrosis was formed. In the second set of experiments, the tissue was sonicated with a chirp difference frequency such that during the 50 msec pulse, the tissue encountered a range of difference frequencies. A chirp frequency sweeps continuously through many frequencies. See section 3.4 for a detailed description of the chirp signal.

In both experiment types, the USAE method relies on the production of two ultrasound beams with slightly varying frequencies. For most of the single frequency experiments, this acoustical field was created by a pair of confocal, co-axial transducer elements which formed a spherically focused annular array. The combined array with an outer diameter of 10cm and a focal distance of 8cm was made of PZT-4 piezoelectric crystal with a natural resonant frequency of 1.7 MHz. The single spherically shaped crystal was divided into two elements of equal area by etching the gold electrode on the back surface of the crystal while keeping the common grounding electrode on the front surface intact. For a few single frequency experiments, and for all of the chirp experiments, a similar transducer was used which was divided into right and left elements as opposed to inner and outer co-axial elements. The right/left element transducer was

made of PZT-4 piezoelectric crystal with a center frequency of 1.62 MHz. The right/left transducer was made in-house by cutting the single spherical crystal into the two elements and re-attaching them with a thin layer of silicone in order to provide superior mechanical isolation of the two elements. The efficiency of the right/left transducer averaged over both elements was 66% while the efficiency of the co-axial transducer averaged over both elements was 72% (see Appendix A).

The electrical impedance of each element of each transducer was matched to 50 Ω using an L-C network. Each piezoelectric crystal element was driven by an RF-amplifier (Electronic Navigation Industry, models 3100L and A150) which was modulated by a frequency generator (Stanford Research Systems model DS345, HP model 33120A, Wavetek Arbitrary Function Generator model 395).

In order to accurately move the transducer during area and line scans of the sample, the transducer was mounted on a 3D positioning system (Velmex, model Unislide) and placed in the tank of degassed water together with the sample being imaged. The low frequency USAE response from the sample was detected by a hydrophone (Benthos Inc., AQ-18) that was also positioned in the water with the sample. The signal from the hydrophone was filtered with a differential amplifier (Preamble Instruments, model 1820) or a digital filter (Stanford Research Systems, model SR 650) to reduce noise and registered with a digital oscilloscope (Tektronix model 2431 L or Tektronix model TDS 210).

Careful system design and special consideration were required to isolate the entire system from external noise. The USAE method relies on small difference frequencies (in the kHz range) making it very sensitive to outside noises from fans, generators, and the

lab environment. All noisy equipment was removed from the room housing the tank and hydrophone, and many scans were conducted at night to reduce background noise. In addition, the scan tank was lined with high frequency acoustical absorbers in order to reduce the system noise from reflection and scattering within the tank.

3.1 Computer control

The pulse timing, data acquisition, and transducer positioning were controlled by a Windows 98 personal computer using a GPIB interface (IEEE 488.1 protocol), the RS232 serial port, and the LPT1 parallel port. The PC interface with the function generators, oscilloscope, and positioning system was also used to set the scan parameters before the scan was initiated. These parameters were recorded as header information in the data file of each scan. The data was acquired from the oscilloscope and each waveform was recorded as binary information to the data file. The control software was written in Basic ver. 7 because the DOS based language has reliable timing with the clock of the Pentium processor. In contrast, other languages written for windows based programming often have timing complications because they have to share resources and processor time with background windows processes. In these experiments, timing down to millisecond accuracy is an important consideration.

In addition to controlling the experiment, a computer was used to post-process the waveform data of the sample's response to each diagnostic pulse. The waveform was saved as a binary file during the experiment and later read into Matlab (ver. 5.2) and processed using algorithms written in the Matlab language according to the scan parameters saved in the header information of the wave data file. The algorithms relied

upon the Matlab FFT function to calculate a fast Fourier transform of the waveform. From this FFT, the amplitude of the response at the frequency of interest was determined. This amplitude of the FFT of the response signal from the object in the scan tank is referred to herein as the USAE amplitude. In future experiments, the data could be processed in real-time by integrating the DOS based scan program and the Matlab code into one application.

3.2 Samples

The samples used in the experiments varied. The specific samples are listed in the results section, but the methods for conducting the experiment were independent of the type of object being sonicated. The purpose of these experiments was to test the applicability of this system for measuring properties of tissue which would be important in monitoring thermal surgery. These include stiffness, absorption coefficient, temperature, and thermal dose. Therefore, the samples used were various types of *ex vivo* tissue ranging from store purchased (and de-gassed) pork and beef, to fresh (less than an hour post-mortem) rabbit and porcine liver, muscle, and fat. In addition, a few scans were run on metal objects to test if the system was operating correctly by determining if there was a response from the metal which is very stiff relative to tissue.
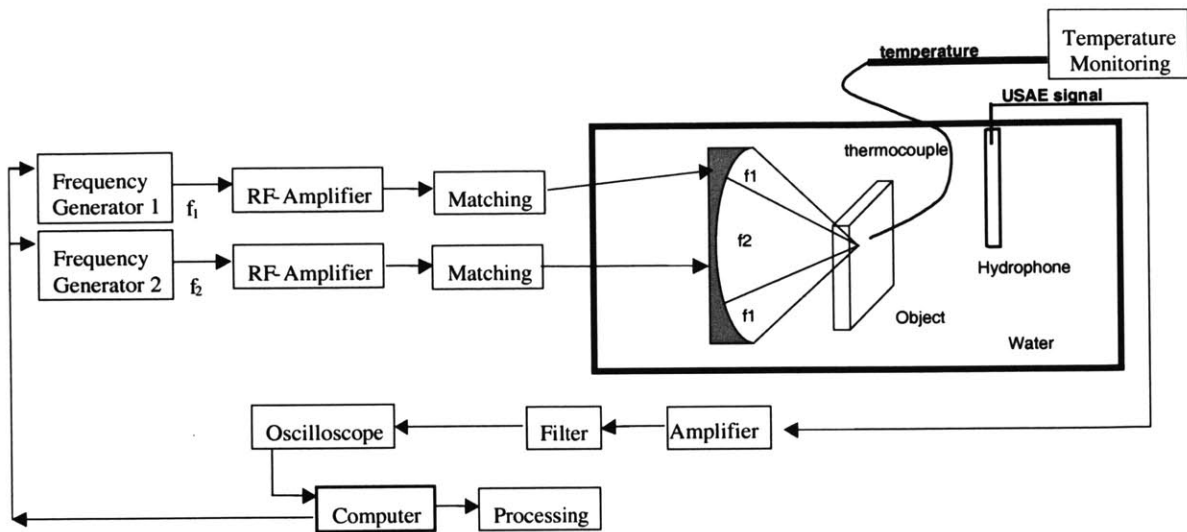
Figure 3-1. Experimental set-up.

3.3 Single Difference Frequency Experiments

In the first set of experiments, a single difference frequency was used to sonicate the tissue. The difference frequency, as described in the theory section (section 2.1), is a low frequency signal formed from the difference of the two high frequency elements of the transducer. For a difference frequency of 7 kHz, one element of the confocal element transducer was driven at 1.7 MHz and the other was driven at 1.707 MHz. Likewise, for a 7 kHz difference frequency, one element of the left-right element transducer was driven at 1.62 MHz while the other element was driven at 1.627 MHz. During the single frequency experiments, only one difference frequency was scanned at a time. The difference frequency used depended on the specific properties of the object being sonicated and the acoustics of the set-up during the experiment. This is the essential

difference between this set of experiments and the later chirp experiments in which each pulse from the transducer contained a ramp of frequencies from the lowest to highest desired difference frequency.

According to the theory of the USAE method, increasing the absorption coefficient after the tissue is necrosed causes the amplitude of the USAE response to increase. However, the increased stiffness of the necrosed tissue will cause the USAE amplitude to decrease. The resulting change in the amplitude of the USAE response after the tissue has necrosed is a complex, three-dimensional mechanical-acoustical problem without a closed-form analytic solution. The stiffness change in the tissue will affect the tissue's frequency response differently because the resonant frequencies and their associated harmonics are stiffness-dependent. Thus, altering the stiffness of the tissue by necrosis will shift the resonance of the mechanical system being sonicated. This shift in the target's resonance along with changes in the acoustic absorption coefficient will cause a change in the USAE amplitude at any difference frequency. At a single difference frequency, this change in the USAE amplitude is not predictable because the system is not easily modeled. In the theory section, a finite element analysis of the system is described which provides simulated responses for various frequencies. However, for the purposes of this section, it is important to note the difficulty in determining the appropriate difference frequency to use for any given scan and the uncertainty in the direction of the change in the USAE amplitude after the tissue is necrosed. A practical solution to these problems is described in the frequency scan section (section 3.3.1). In the second type of experiment conducted, the technique of 'chirping' replaces single

frequency scanning, thereby offering another solution to the difficult problem of selecting the optimal scan frequency.

3.3.1   Frequency Scan

In order to determine the optimal single difference frequency to use for USAE diagnostic pulses, a frequency scan was first performed on a test portion of the target object. For measuring tissue necrosis, the frequency scan was run before and after the tissue was necrosed. The relative increase or decrease was observed at each difference frequency in the scan to determine an optimal frequency at which the necrosis caused a large change in the USAE amplitude. This optimal difference frequency was then used as the single frequency in later scans of the same object. The majority of frequency scans ranged from 1 kHz to 20 kHz by 50 Hz or 100 Hz steps because this range of difference frequencies provided the greatest amplitude USAE response.   Above 20 kHz the amplitude falls sharply due to the decreased sensitivity of the hydrophone above 20 kHz as well as the decreased response amplitude of the system at higher frequencies based on the mechanical resonance of the system. A similar effect is noted for the finite element simulations (Figure 2-9). The pulses at each frequency lasted 100 msec and were spaced 1 second apart. Although the amplitudes, pulse duration and scan frequencies differed slightly from experiment to experiment, the basic procedure remained the same for each frequency scan.

3.3.2   Single Location Scan

After establishing an optimal difference frequency for a given sample based on the frequency scan, the sample was scanned in a new location at its optimal frequency. For a single location scan, the tissue sample was sonicated at the optimal difference frequency for a short duration on the order of 100 msec (this varied slightly per experiment) several times to get an average UASE amplitude value. Next, the tissue was sonicated at high power (25-75 W) for 30-60 seconds in order to create a lesion of necrosed tissue. Finally, the USAE pulses at the difference frequency were repeated to get an average value of the USAE response after necrosis.

3.3.3   Area and Line Scan

In some samples, a line scan or an area scan was conducted to obtain a series of USAE amplitudes at various positions in the object. In order to obtain a line or area scan, the transducer was physically stepped in a raster pattern through each position by the Velmex Unislide three-dimensional positioning system. At each position, the Velmex system paused for one second while the transducer was pulsed at the optimal difference frequency for a short (100-250 msec) pulse duration and the Tektronix oscilloscope transferred the waveform to a data file on the computer. The data from a line or area scan was post-processed in Matlab in the same manner as a frequency or single location scan. However, in the case of a line or area scan, the data was displayed as an image such that the value of each point in the one-dimensional or two-dimensional image was equal to the amplitude of the difference frequency as calculated by an FFT of the response waveform.

3.4 Chirp Frequency Experiments

The second series of experiments used a chirp signal instead of a single difference frequency signal. Although the results from scans using a single difference frequency were promising, the single frequency scans had several limitations. These include the inability to know beforehand which difference frequency would be optimal for performing single location and line or area scans. The solution to this problem was to perform a frequency scan in each sample at a different location before and after necrosis and to select the optimal frequency using this preliminary frequency scan experiment. This solution proved adequate in many, but not all, experiments. The frequency scans were uninformative in some experiments because as hypothesized and demonstrated by the simulations in the theory section, the amplitude of the response is highly dependent on the physical parameters of the system. These parameters include the thickness of the sample, its exact mechanical properties, its boundary conditions, and the location of the lesion in the sample. These parameters are obviously different for the location of the frequency scan and the location of the subsequent scans in the same sample. In addition, choosing a single difference frequency may be limiting, only giving a partial picture of the response, because no response information at other frequencies is acquired.

It would be best to measure the response at many difference frequencies in order to provide more information about the characteristics of the system. For example, if tissue necrosis caused a frequency shift of the sample's resonant frequency, the shift would go undetected through sonicating and recording the response at a single difference

frequency. A frequency shift of the sample's resonant frequency would appear simply as an increase or decrease in the amplitude when measured by only a single frequency. A frequency scan would provide information about the system's harmonics (as described above in section 3.3.1) by recording the response to each difference frequency separately, one after the other. Each scan however, takes 25-60 minutes and is therefore prohibitively time-consuming. The long duration of this type of scan increases the likelihood that system-sensitive tissue properties and experimental parameters will fluctuate. It is not ideal to measure the response of tissues or other samples via a single difference frequency because it is difficult to determine which difference frequency to use beforehand. Also, narrowing the scope to a single frequency confines the extent of the analysis by limiting the information obtained about the sample. However, taking an entire frequency scan is not feasible because it takes so long that it is impossible to ensure that the system parameters have not drifted over the course of the scan. Additionally, a time consuming frequency scan is not practical for clinical use because it requires the patient to lay perfectly still for an extended period of time.

The solution to these limitations of the single difference frequency experiments is to use a chirp function rather than a pulse at a single function. A chirp, otherwise called a sweep function, is a single sinusoidal function of a finite duration and with a time varying frequency. In a sense, it is equivalent to performing a frequency scan condensed into a single pulse with a duration on the order of milliseconds. The chirp function used in the following experiments was created by a WaveTek arbitrary waveform generator and spanned 1 kHz to 20 kHz over the duration of 50 msec. The function generator used 99 steps to span this frequency range, thereby effectively stringing together 99 partial

43

sinusoids ranging in frequency from 1 kHz to 20 kHz in steps of 200Hz to form one continuous sinusoid lasting 50 msec.

The chirp function was utilized exactly as the single difference frequency had been used in the above experiments. In the case of the chirp, one element was pulsed for 50 msec at its center frequency while the other element was chirped through all 99 frequencies in the same time period. A single 50 msec pulse of the chirp method showed results equivalent to a 30-minute long frequency scan as described in the single frequency method above.[4]

The chirp method enables the experiments to be conducted much more quickly because it eliminates the need for a preliminary frequency scan to determine the optimal frequency. This is because information from the response to all frequencies in the range are measured. The additional information the chirp method provides in such a short time (50 msec) makes possible many other types of measurements.

3.4.1 Single chirp Scans

The most basic chirp scan performed was the single chirp over the frequency range 1kHz to 20kHz. The response was recorded for several repeated chirps before

---

[4] It is important to note that a chirp is not the same as a broadband burst. A broadband tone burst is often used to determine the resonant frequencies of a system in a different manner. It is a single pulse containing the sum of many different frequency sinusoidal waves added together on top of one another in parallel. Each sinusoid spans the duration of the entire pulse. In contrast, the chirp is a single sinusoidal wave which varies in frequency as a function of time. The chirp appears as a sinusoid compressed continually with time such that the peaks of the wave are progressively closer together at later times. It is analogous to adding many different frequency sinusoids together end-to-end, in series. In this way, the sample is sonicated by each difference frequency of the chirp individually one after the other, as a function of time, rather than all difference frequencies simultaneously as in a broadband pulse. Because the sample encounters each difference frequency sequentially, it responds to each frequency sequentially. In this way, the sample's response to the lower chirp frequencies is found in the first portion in time of the response waveform while its response to the chirp's higher frequencies is found later in the response waveform.

sonicating the tissue to create a lesion, and again after the lesion had been formed. The waveforms from the chirps were recorded and post-processed in Matlab in a similar method as described in the single frequency scans by taking an FFT to observe the frequency content of the response. In the case of the chirp, the FFT looked almost exactly like the time domain response signal itself. The reason is apparent when considering that the sample responds with a given amplitude at the same difference frequency with which it was sonicated. Thus, the amplitude at each instant in the time domain response signal represents the amplitude of the sample's response to the corresponding difference frequency at that time. In other words, the early portion of the response in the time domain represents the response at the lower frequencies, while the latter portion of the response in the time domain represents the response at the higher chirp frequencies. Therefore, the time domain response signal will closely resemble an FFT: a calculation of the frequency content of the signal. This is because both represent the amplitude of the response at each frequency.

3.4.2 Line Scans

Line scans were conducted in a manner identical to the case of a single difference frequency. The same stepper motor positioning system was utilized to move the transducer to each new location at which it emitted a chirp rather than a single frequency pulse.

3.4.3 Temperature Scans

In these scans, the relationship between the USAE response and temperature was analyzed by heating and cooling the sample while recording the waveforms of the response to a chirp. In the heating phase of the scan, the element to remain at the center frequency was sonicated continuously in order to heat the sample at the focus, while the second element was chirped every second and the response recorded. In the cooling portion of the scan, both elements were pulsed once per second (allowing the sample to cool), and the response of each pulse was recorded. These scans were performed at several locations in each sample. At the first location in each sample, a calibrated thin wire, copper-constantan thermocouple was located at the focus to record the temperature change as a function of time (and USAE pulse number). This temperature-time curve was used for comparison for all temperature scans in the same tissue because the heating properties of tissue are fairly constant in a given sample. In addition, it was important to make measurements without a thermocouple at the focus to eliminate the effects that the metal wire itself might have on the USAE response. Temperature scans were conducted at several different power levels in each sample to observe the effects of higher heating and higher signal-to-noise ratio for higher amplitude power levels. The following table shows the power levels used for the temperature experiments.

Wavetek Arbitrary Waveform Generator Voltage with 55 db ENI Amplifier (Volts)	Stanford Function Generator Voltage with 50 db ENI Amplifier (Volts)	HP Function Generator Voltage with 50 db ENI Amplifier (Volts)	Electrical Power Output for Each Element (Watts)	Total Electrical Power for Transducer (Watts)	Total Acoustical Power for Transducer (Watts)
.058	.100	.100	2.2	4.4	2.9
.085	.125	.125	5	10	6.6
.105	.200	.200	8	16	10.56
.137	.250	.250	13	26	17.16

Table 3-1. Power levels used during chirp temperature scans.

4 Experimental Results and Analysis

4.1 Single Difference Frequency Experiments

4.1.1 Frequency Scan

The following example of a frequency scan represents a typical scan of this type. The focus remains at a single location in fresh, *ex vivo* rabbit liver for the entire scan. The frequency scan ranged from 6-13 kHz difference frequency with .05 kHz step size. The dotted line is the amplitude of the USAE response (averaged over four repeated scans) at the difference frequency measured before the lesion was formed. The solid line is the same measurement made after the lesion was formed. Notice that in some places, the USAE signal is shifted up in amplitude after the sonication.
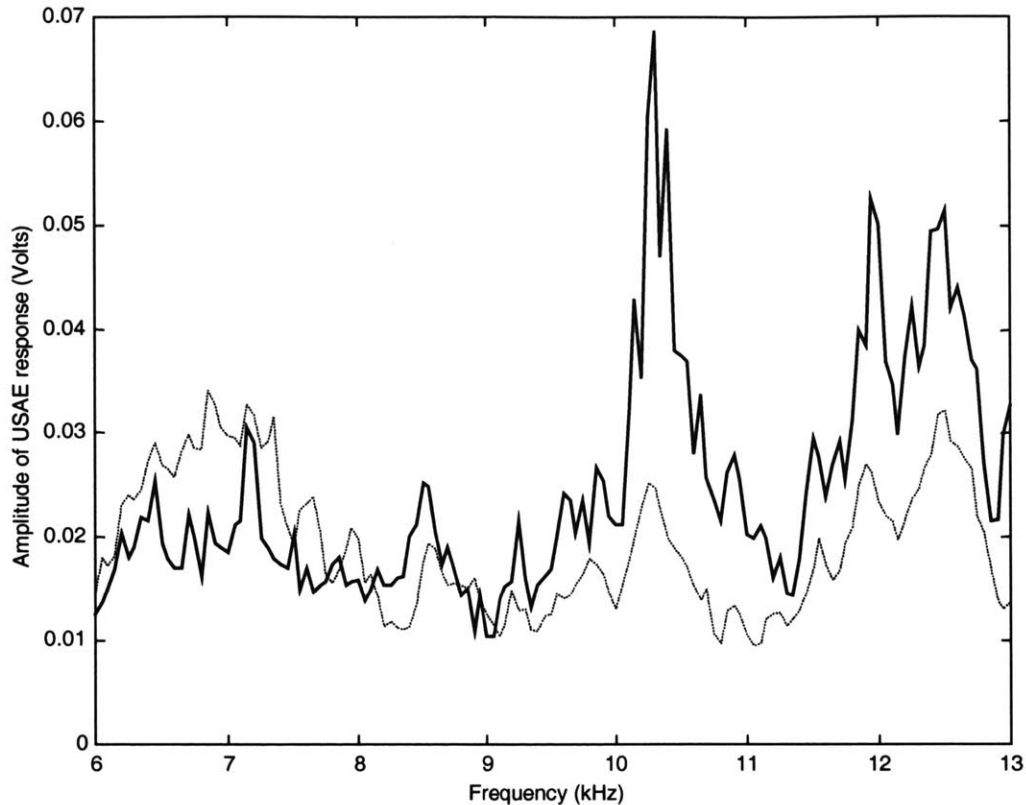
Figure 4-1. Frequency scan of a single point in *ex vivo* rabbit liver from 6-13 kHz difference frequency with .05kHz frequency step size. Measurements are made before lesion is formed (dotted) and after lesion is formed (solid).

This scan demonstrates an increase in the amplitude of the USAE signal at many frequencies after forming a lesion, but this does not hold true at all frequencies. Notice that at lower frequencies in this scan, the post-lesion USAE amplitudes are actually lower than the pre-lesion amplitudes. This discrepancy was expected after carefully considering the system's mechanics and verified using finite-element simulations. This example demonstrates that the shift is USAE amplitude after necrosis is unpredictable, and calls for a frequency-independent or optimal frequency method for scanning the tissue. Results of this nature in the single frequency method motivated the switch to the

chirp method described in the second set of experimental results. The frequency scan was not always adequate for selecting this optimal difference frequency to perform single location and area/line scans because the mechanics of the entire system change for each new location in the sample. In this case, 10.3 kHz was selected as the optimal difference frequency for line and area scans. However, in a new location in the same sample, this may not actually prove to be a good difference frequency for distinguishing between the pre- and post-necrosed tissue. The single frequency experiments provided very interesting results when the correct difference frequency was chosen. For many experiments, the preliminary frequency scan like this one proved a sufficient technique for selecting the difference frequency.

Below, a frequency scan from a fresh liver sample of another rabbit shows the before and after USAE amplitudes at various difference frequencies. In this sample, the peak difference was found to be at a difference frequency of 18.7 kHz. Again, notice that at other frequencies (13-15 kHz) the frequency scan before the lesion is formed is actually greater in amplitude than the one conducted after the lesion is formed. This data is averaged over 6 frequency scans before and after the lesion was formed.
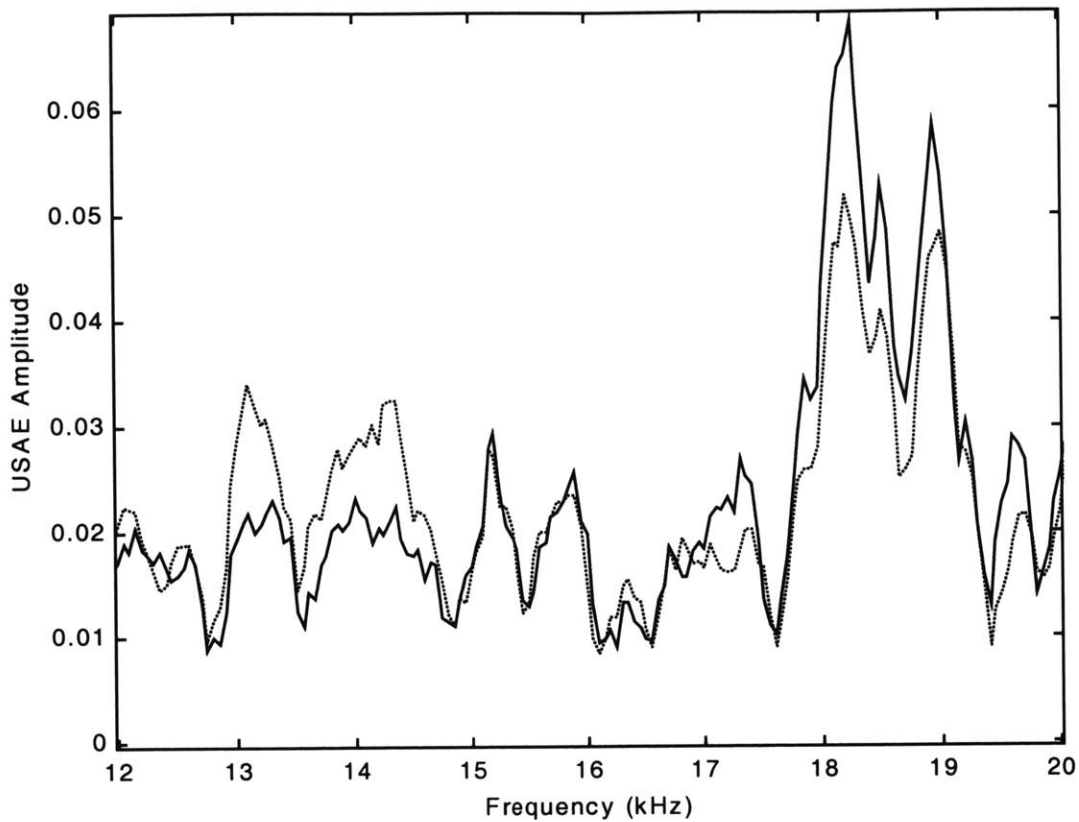
Figure 4-2. Frequency scan in *ex vivo* rabbit liver averaged over 6 measurements before (dotted) and after (solid) a lesion is created.

4.1.2 Single Location Scan

After the optimal frequency was selected from a preliminary frequency scan, a single location scan was performed to detect necrosed tissue. The following experiment conducted in fresh rabbit thigh muscle demonstrates the ability to distinguish between necrosed and healthy tissue at a single point in the sample. In this experiment, five locations in the rabbit thigh muscle were sonicated with a diagnostic USAE pulse with a difference frequency of 12 kHz before and after a lesion was formed. In order to weigh the USAE value against background noise and variation in the amplitude of the response,

the measurement was repeated five times at each location before and after the lesion was formed. The lesions were all formed in the same manner by sonicating at higher power, 25.2 W continuous wave, for 30 seconds. Each pulse lasted 30 msec and was repeated every 2 seconds in order to allow the system to settle from the diagnostic pulse. The five locations in the thigh muscle were sonicated with a different amplitude USAE pulses in order to simultaneously determine the optimal power levels for use with the USAE system. Lesions one through five used .066 W, 3.3 W, 12.54 W, 23.1 W, and 33 W total acoustical power respectively. Figure 4-3 shows the USAE amplitude (at a difference frequency of 12 kHz) averaged over five measurements and the corresponding standard deviations.
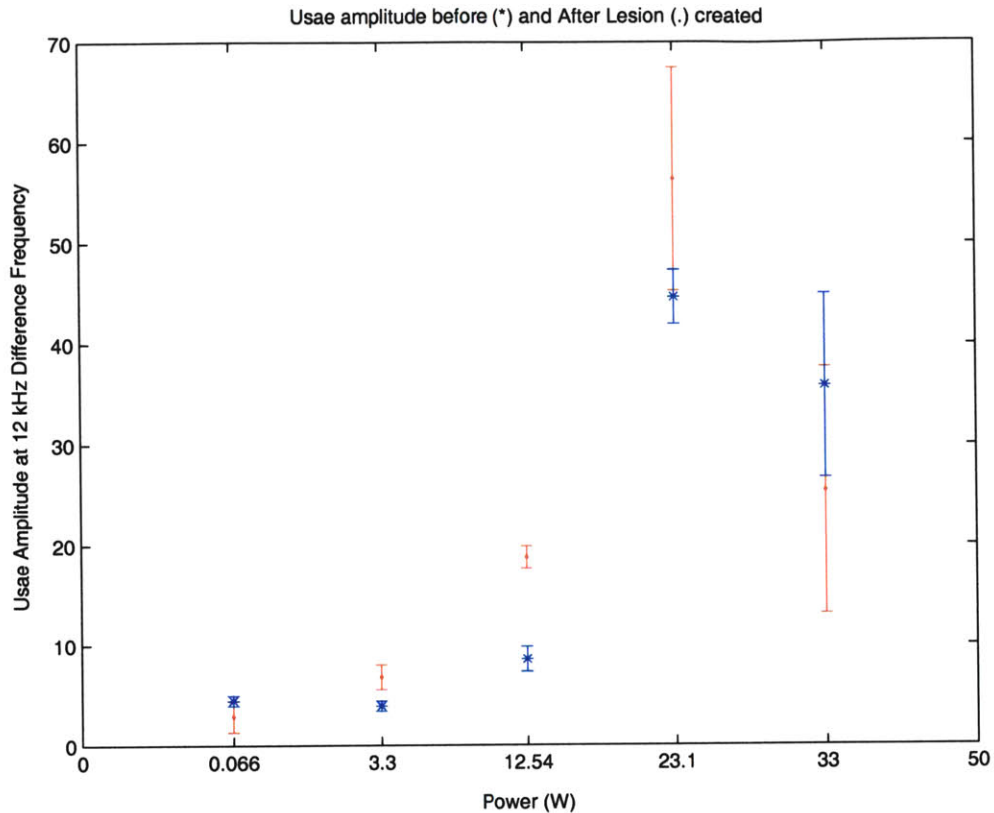
Figure 4-3. Average USAE amplitude before (*) and after (.) a lesion was created. Plotted +/- one standard deviation. USAE measurements made from pulsing each lesion at a different USAE power level.

This series of experiments demonstrates the distinction between the amplitudes of the USAE signal before and after a lesion is created in the case of lesion 3 which used a USAE pulse amplitude of 12.54 W acoustical. For lower power diagnostic pulses, the amplitudes of the response are not large enough to overcome the noise level of the system. For this reason, the .066 W pulse responses before and after the lesion is made are indistinguishable. Similarly, the 3.3 W pulses are barely distinguishable. At lesion 3 (12.54 W), the amplitudes are large enough to rise above the noise level. This is evident by the statistical difference between the before and after responses, and also by the rise in the amplitude of the before response compared to responses at lower power level pulses.

In lesions 4 and 5, the power levels used are 23.1 W and 33 W respectively. These large power levels are likely to cause cavitation in tissue. Although cavitation is not proven in this case, the large standard deviation of the responses in these two lesions demonstrates the erratic nature of the USAE response which is a characteristic of tissue with cavitating air bubbles. Further evidence of large USAE amplitude fluctuations during cavitation events is presented in the temperature section of the chirp experiments presented below (section 4.2.4). This experiment demonstrates both the ability to detect necrosed tissue and also the sensitivity of the measurements to the power levels used. If the power is too low, the response signal is lost in the noise. If the power is too high, the USAE pulse may cause cavitation which can dramatically affect the response signal, and mask useful information which might have been obtained.

4.1.3   Area and Line Scan

4.1.3.1   U-shaped Metal

Preliminary experiments were conducted on a U-shaped piece of metal because its mechanical properties are so different than those of water that it is an ideal candidate for testing and calibrating the USAE system. The metal was first sonicated using a line scan with a frequency spectrum taken at every position in the scan. The scan crossed both legs of the metal target for a total distance of 20 mm in the X-direction. The step size used was .5 mm. At each position of the line scan, a frequency scan was performed from 1 kHz to 100 kHz with a step size of .5 kHz. The frequency scan was performed to discern the frequency dependence of the response and to help select an optimal frequency for use in a larger area raster scan of the sample. This method offers more information than

simply conducting a frequency scan at a single point (as done in the case of the rabbit liver samples above). However, this line-frequency scan took many hours to complete because it required so many pulses[5]. This type of scan would not be possible in the case of fresh rabbit liver because the liver quickly decomposes post-mortem and the mechanical and acoustical properties would change over the course of such a long scan. The chirp method offers a way to acquire this information in a very short time frame, ideal for time sensitive experiments.
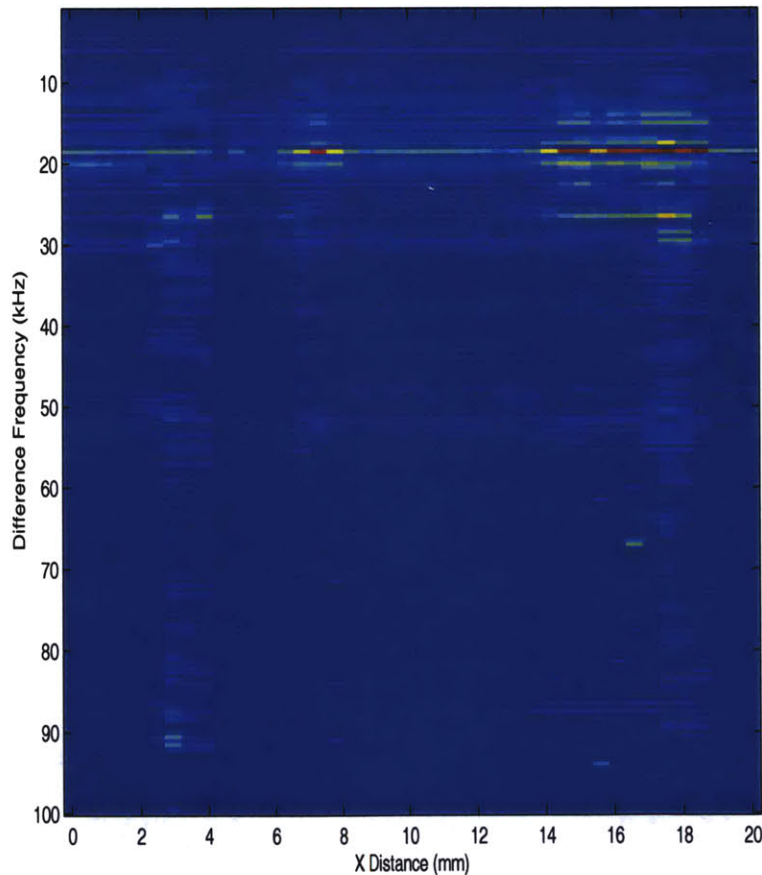
Figure 4-4. Line scan across legs of U-shaped metal over a range of difference frequencies.

___

[5] (41 points in the line scan) x (199 points in the frequency scan at each location) = 8159 pulses total

This line scan across the two legs of the metal reveals the geometry of the target. The increased amplitude of the USAE response is observed at several frequencies when the transducer is located at the X-position of the metal legs. After observing the response from the line scan across frequencies from 1 kHz to 100 kHz, a difference frequency of 10 kHz was selected for use in an area scan. Although the response from the line-frequency scan above appears to be greatest in the range of 16 kHz to 20 kHz, there is significant response from the water alone in this frequency range as indicated by the amplitude of the response from between the two legs of the metal object (at x = 10 mm). This is most likely due to resonance of the physical system, including the tank walls and hydrophone casing, at these frequencies. Thus, the signal-to-noise ratio is not as large here as it is at other frequencies. The USAE response from the fork is much larger than the background response of the water at any frequency from 1 kHz to 100 kHz aside from this small span of resonance frequencies. The change in amplitude when positioned on the metal legs is due to the impedance mismatch of the metal which causes a large reflection coefficient. The large reflection coefficient in turn causes a large incident radiation force on the sample.

The U-shaped metal was scanned at 10 kHz in a raster pattern of 20 mm by 20 mm. In the x-direction (width), the step size was .25 mm. In the y-direction (height), the step size used was .5 mm. Figure 4-5 displays the image created by plotting the amplitude of the USAE response at 10 kHz for each X and Y coordinate along with a photograph of the metal target.
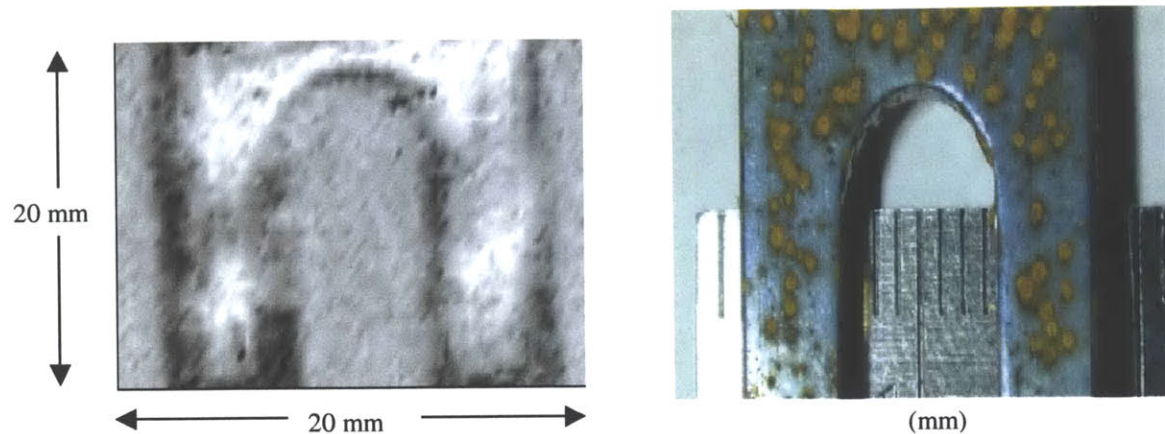
Figure 4-5. USAE image (left) and photograph (right) of U-shaped metal target.

4.1.3.2 Rabbit Liver

Imaging tissues is far more challenging than imaging metal objects because the property changes after necrosis are much more subtle than the distinct properties of metal. In addition, as described in the theory section, the increased stiffness and increased absorption both characteristic of necrosed tissue work against each other in terms of their effects on the amplitude of the USAE response. Nonetheless, images of fresh tissues were successfully acquired with this system.

Below, images of a 10mm by 10mm area of fresh, *ex vivo* rabbit liver were formed by scanning with a USAE difference frequency of 10.3 kHz in a raster pattern. The raster pattern was created by mechanically stepping the transducer through a 10mm x 10mm grid with a step size of .5mm. This example of an area scan was taken from the same liver sample as used in the above frequency scan example (Figure 4-1). The 10.3 kHz difference frequency was selected for the area scan because it demonstrated the

greatest increase in USAE amplitude as measured in the before and after frequency scans depicted above (Figure 4-1). The first image on the left was scanned before the lesion was formed. The lesion was created by sonicating at a power of 18 W acoustical for 20 seconds. The middle image was scanned after the lesion of coagulative necrosis was formed. The final image on the right is a photograph of the lesion created at the focus taken after the tissue had been dissected in the plane of the focus.
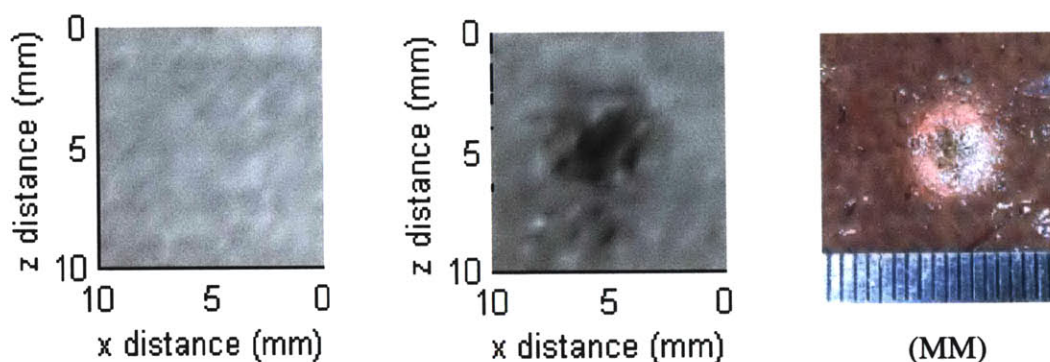
Figure 4-6. USAE image before lesion formed (left), after lesion formed (center), and photograph of lesion (right) in fresh rabbit liver *ex vivo*.

In another example, an area of 30mm by 30mm was scanned with the USAE method after a pattern of necrosis had been formed from a high power sonication to the tissue. This is a sample of fresh, *ex vivo* rabbit liver taken from a different animal than the liver used in the above example. Two bands of necrosis and two point lesions were created in the liver by moving the transducer slowly while sonicating at high power, causing tissue necrosis. The step size of this area scan was .5 mm in each direction. The results below are obtained from averaging the USAE amplitude over four measurements acquired at each location.
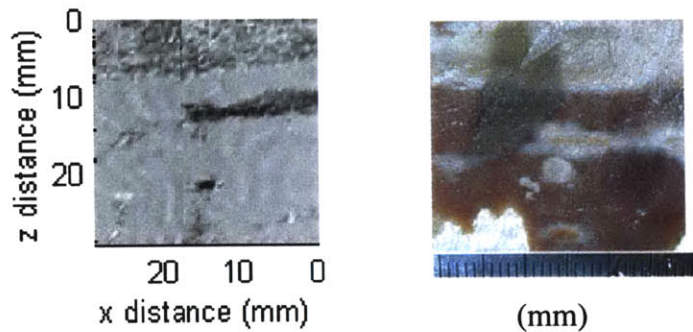
Figure 4-7. USAE image of necrosis pattern (left) and photograph of necrosis patter (right) in fresh rabbit liver *ex vivo*.

4.2 Chirp Frequency Experiments

4.2.1 *Single chirp Scans*

Experiments with the chirp technique proved successful. This technique produced results similar to the single frequency experiments, but chirp scans offered more frequency information than single frequency scans. The frequency spectrum below depicts the increased amplitude of the USAE response to a chirp signal before and after a lesion was created. The sample used in this experiment was fresh porcine thigh muscle. The data is averaged over three pulses before and three pulses after the lesion was formed. The plot appears to resemble the frequency scan at a single frequency described above in the single frequency experiments (section 3.3.1), but the data was acquired after a single chirp pulse, rather than consecutive pulses at each difference frequency. The plot is the FFT of the response to the single chirp pulse and it indicates the relative contribution to the response of all frequencies from 0 to 25 kHz, where 25 kHz is the

58

Nyquist limit of the FFT. Notice that there is no contribution to the response from frequencies below 1 kHz or above 20 kHz. This is because the chirp signal sent to the sample ranged only from 1 kHz to 20 kHz. This fact supports the theory that the response to each distinct frequency in the chirp is at the same individual frequency as that portion of the USAE chirp signal itself.
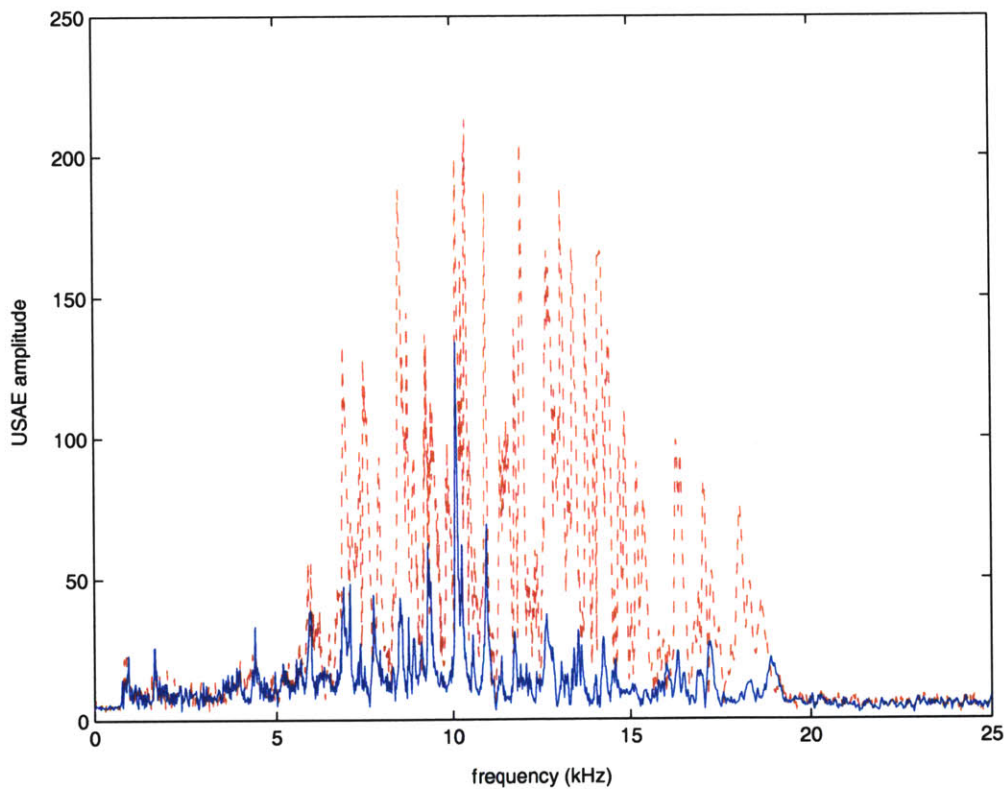
Figure 4-8. USAE amplitude response to a chirp before (solid, red) and after (dashed, blue) a lesion is formed in fresh porcine tissue *ex vivo*.

4.2.2 Line Scans

The following line scan performed in fresh porcine thigh muscle demonstrates tissue necrosis imaged using the chirp method. The line scan ranged from 0 to 20 mm with a step size of 1 mm. The data is averaged over three chirp pulses per position in the line scan before and after forming a lesion at the center of the scan (y=10mm). The chirp response is recorded to a data file and is processed by taking its FFT. The FFT is then averaged over the number of pulses recorded for each location. Next, the mean of the FFT from the response before the lesion is formed is subtracted from the mean of the response after the lesion is formed at each location in the line scan. The resulting difference in mean of the FFTs at each location is plotted below.

The lesion is clearly visible between 8mm and 14mm and the response is most pronounced in the 14 kHz frequency range. The measurements of the lesion as imaged with the USAE chirp method correlate well with the actual lesion dimensions shown in the photograph of the lesion taken after dissection of the focal plane.
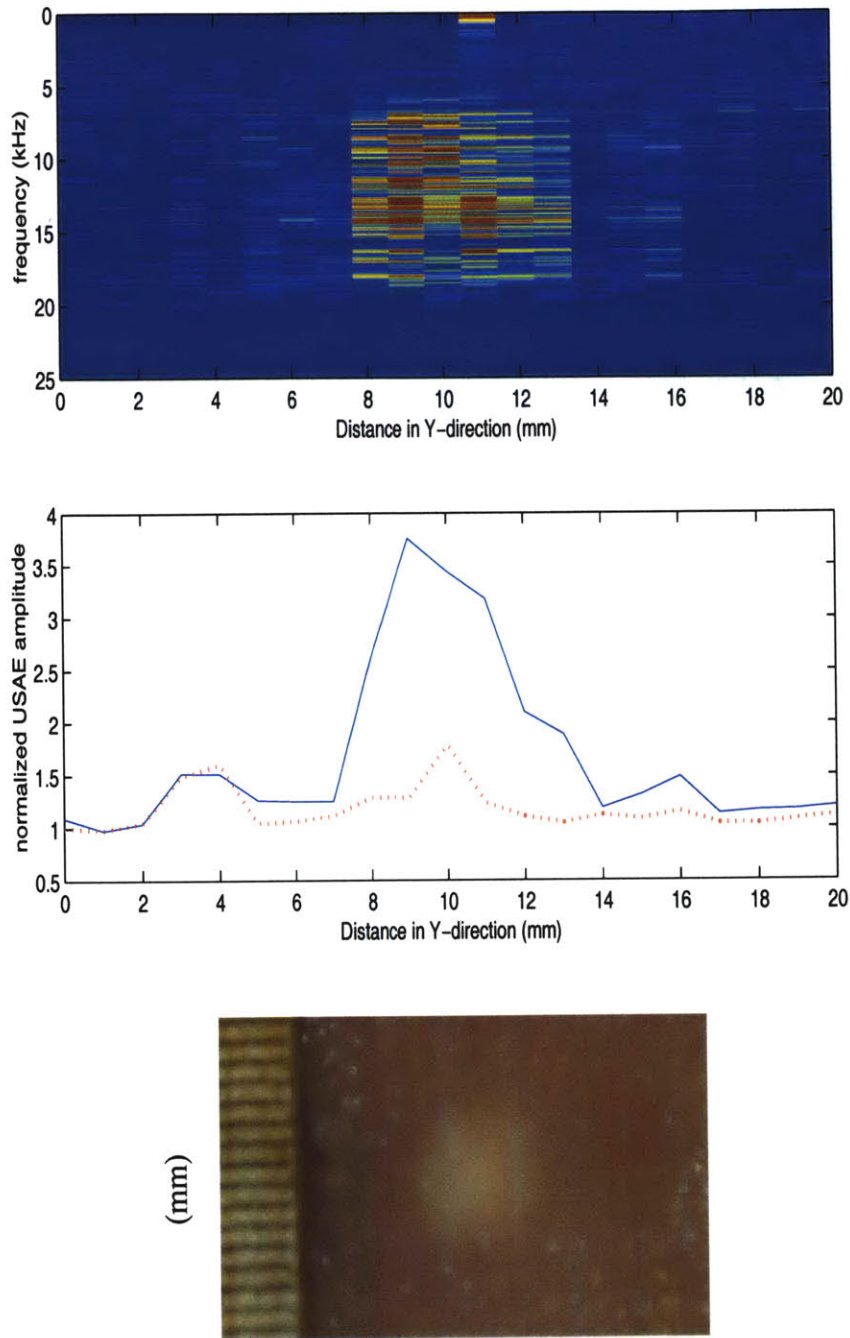
Figure 4-9. Difference between FFT of line scan made before and after lesion is formed at y = 10mm (top); summed amplitude vs. distance for before lesion (dotted) and after lesion (solid) (middle); photograph of lesion (bottom).

4.2.3 Temperature Scans

4.2.3.1   Fresh Porcine Fat

The precise relationship between the USAE response and the tissue temperature is not clear. However, as shown by scans in fresh porcine fat and muscle, the amplitude of the USAE response appears to rise and fall with temperature. An example below is representative of data from scans of fresh porcine fat tissue.

In this experiment, the tissue is heated at three different power levels (2.9W, 6.6W, and 17.2 W acoustic power) in order to bring the tissue to three different temperatures over the duration of each heating period. The heating duration of the low and medium power level scans is 100 seconds followed by a 100 second cooling period. For the high power level scan, the tissue is only heated for 60 seconds in an attempt to avoid cavitation. However, in this case, the tissue appears to have cavitated despite efforts to control this effect. The cavitation section that follows (section 4.2.4) articulates the reasoning behind the conclusion that the tissue in the third scan indeed cavitated. During both heating and cooling, the tissue was sampled with a 50 msec chirp USAE pulse every 2 seconds. The tissue was heated and cooled at each of the three power levels in the same location so that the relative amplitudes of the USAE responses could be compared for each scan in the same location. It is hypothesized that the first two lower power scans produced no irreversible damage to the tissue because the final temperature of the tissue was relatively low and the duration of heating relatively short. The result of the high power scan (and the subsequent cavitation) was a lesion at the

62

focus of the transducer. Note that as a percentage of the base value, the temperature and USAE amplitude increases are roughly equal. It is also significant that the tissue cooled to the same base value at which it started in both temperature and USAE plots.
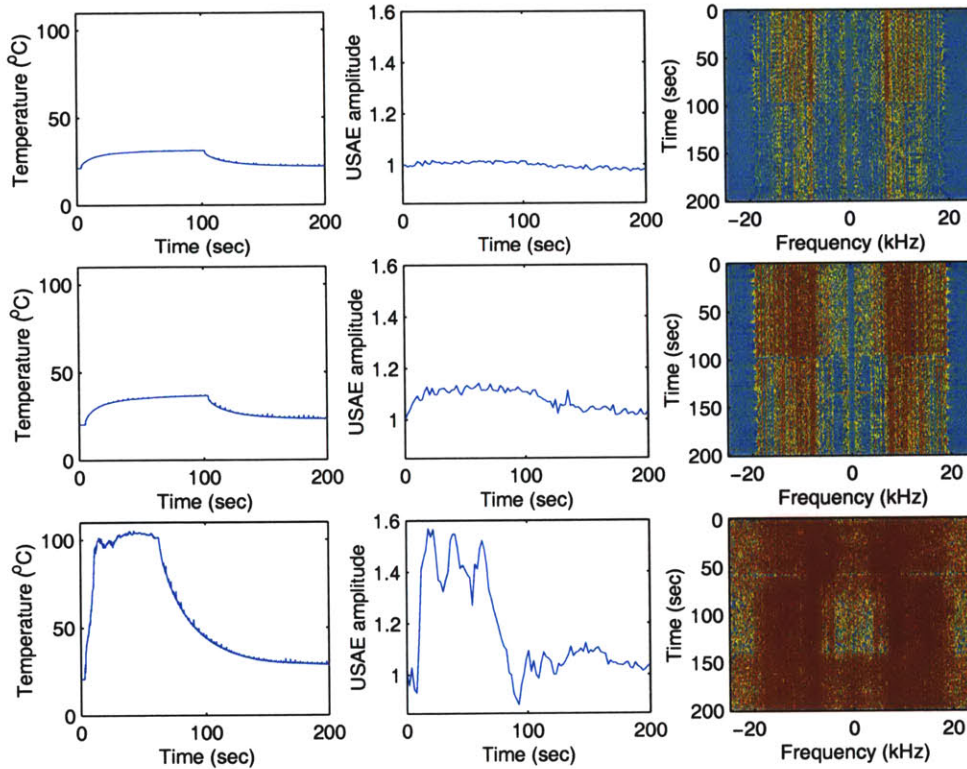
Figure 4-10. Heating/cooling scans at three power levels (row 1= 2.9W, row 2 = 6.6W, row 3 = 17.2W). The temperature as measured with a thermocouple (left column), the summed USAE amplitude (middle column), and the entire frequency spectrum of the USAE response (right column) is plotted.

In this temperature scan, the USAE amplitude represents the amplitude summed over all FFT response frequencies. This attempt to calculate a frequency-independent parameter to measure the USAE response proved successful in many temperature plots. It is effective because the USAE amplitude seems to either increase with temperature or

not change much at all depending on the difference frequency used. Therefore, adding the amplitudes over all frequencies simply averages the change over those frequencies that were affected by the temperature and those that were not. While an optimal frequency range could be determined and used for each experiment, this summed amplitude offers a frequency-independent method for viewing the temperature effects on the USAE amplitude.

In another experiment in fresh porcine fat from a different animal, the tissue was sonicated at a power level between the medium (6.6 W) and high (17.2 W) powers used above. In this experiment, the sample was sonicated at 10.6 W total acoustical power for 10 pulses of baseline measurements, 30 pulses during which it was heated, and 60 pulses during which it cooled. In the top image, the data is presented across all frequencies to show the frequency dependence. In the middle plot, the USAE amplitude is summed over all frequencies and plotted as a function of time to show the temperature dependence. The bottom plot displays the temperature as measured with a thermocouple.

Although plotting the summed amplitude across all frequencies does not always show such a strong temperature dependence, for this example, the smooth exponential rise and fall of the summed USAE amplitude is evident. In other cases, this dependence is weak when the summed amplitude measurement is used. Instead, plotting a summed amplitude over a smaller frequency range is necessary to show the relationship between the amplitude and temperature. Finding the frequency range over which the amplitude responds with temperature is similar to the finding the optimal frequency at which the amplitude responds with necrosis as described in the single frequency section above (section 3.3.1). However, the chirp method often yields encouraging frequency-

independent results such that a total sum across all frequencies suffices to show the signal's temperature dependence.
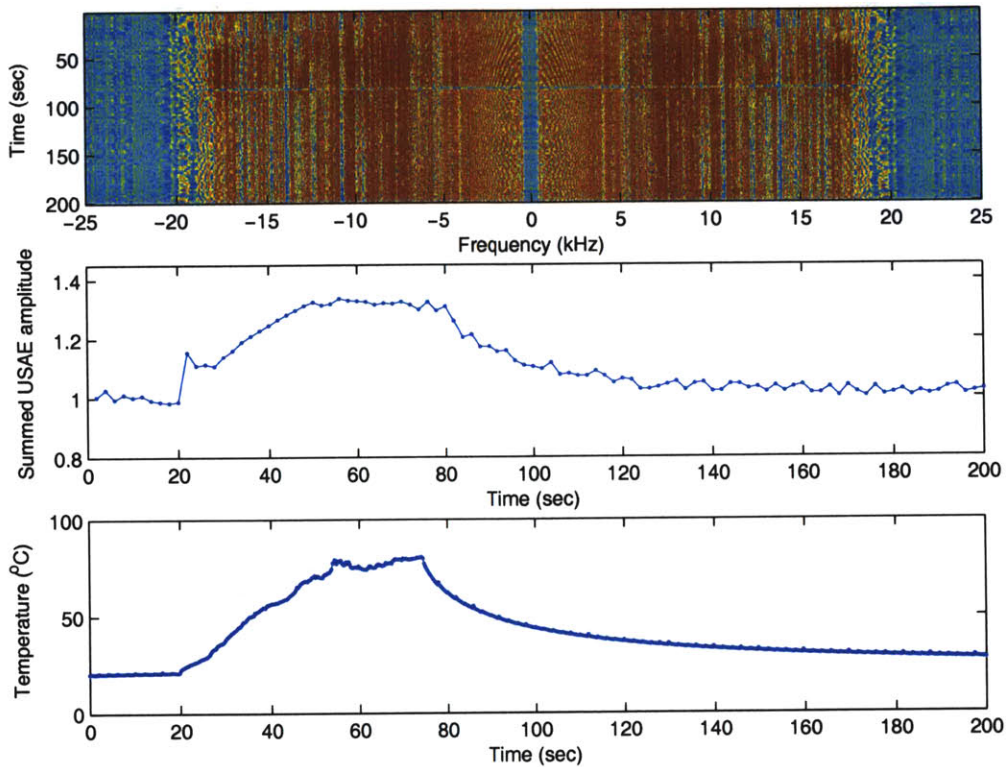
Figure 4-11. USAE response spectrum (top), summed USAE amplitude (middle), and temperature (bottom) during heating/cooling in fresh porcine fat *ex vivo*.

4.2.3.2   Fresh Porcine Muscle

Experiments with fresh porcine muscle also yielded encouraging results for temperature measurements. The muscle tended to have a higher cavitation threshold than the fat and was therefore sonicated at higher powers without demonstrating characteristics of cavitation. The result of this increased amplitude USAE pulse was a

smaller signal-to-noise ratio and experiments which were more repeatable in the same tissue. Below, the average and standard deviation of two temperature plots in fresh porcine muscle are plotted. These scans used 1 high power UASE diagnostic pulse (17.2 W) every 2 seconds for 20 seconds of baseline measurements, 164 seconds of heating measurements, and 316 seconds of cooling measurements. The change in the exponential slope of the temperature curve at t=100 seconds may be due to coagulative necrosis which would cause an increase in the acoustical absorption coefficient and thus an increase in the energy absorbed. This may account for the sudden change in the USAE response from an exponentially rising curve for $t \leq 100$ seconds to a linearly increasing amplitude after t = 100 seconds.
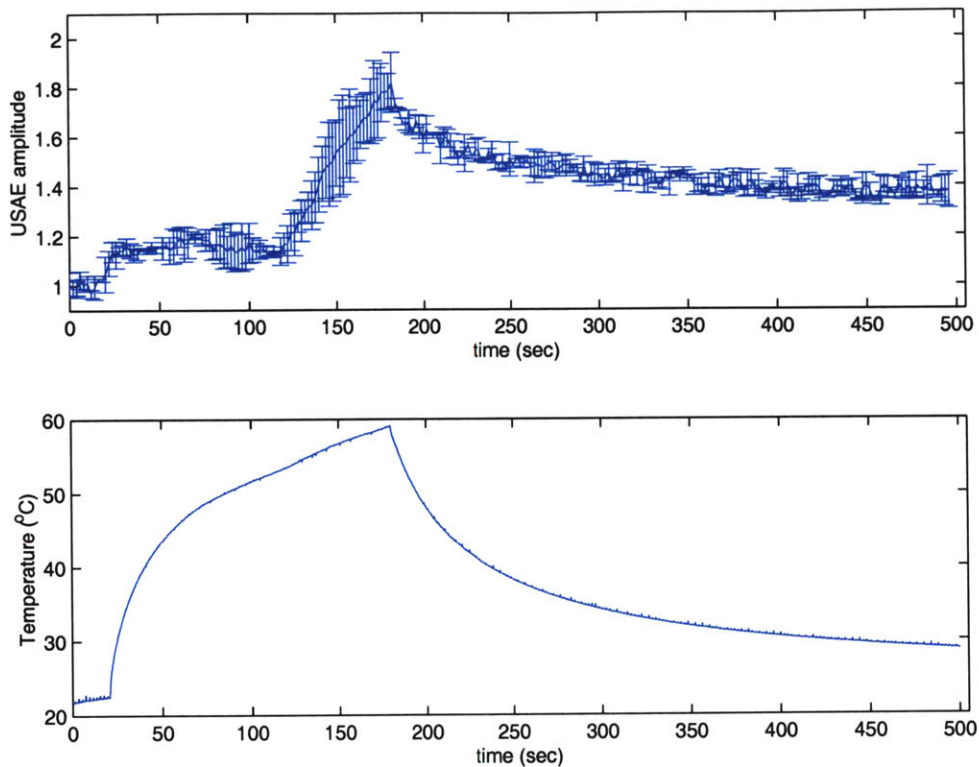
Figure 4-12. USAE summed amplitude (top) and temperature (bottom) during heating/cooling in fresh porcine muscle *ex vivo*.

In another example from fresh porcine muscle of a different animal, an optimal frequency was found by analyzing the response over the entire range of difference frequencies. Although there was some temperature dependence of the summed USAE amplitude over all frequencies, this example shows that choosing an optimal frequency range offers a superior correlation between amplitude and temperature.

This scan used 1 medium power UASE diagnostic pulse (6.6 W) every 2 seconds for 20 seconds of baseline measurements, 200 seconds of heating measurements, and 380

seconds of cooling measurements. The optimal frequency range over which the USAE amplitudes were summed spanned 6100 Hz to 6200 Hz.
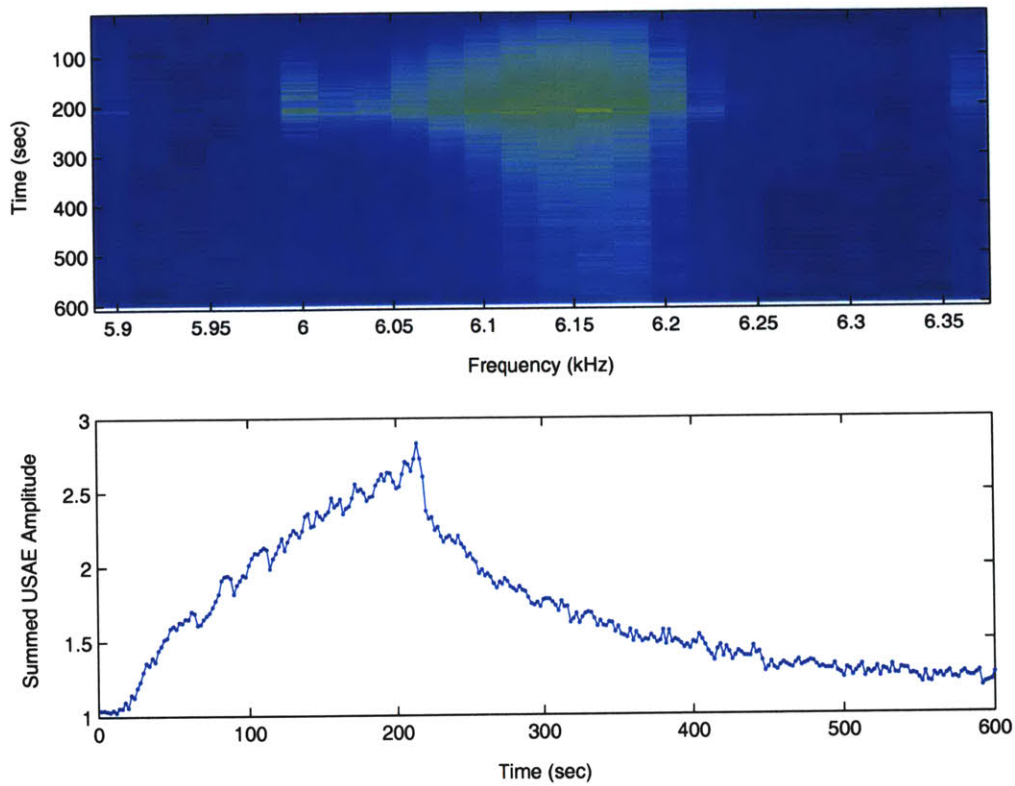
Figure 4-13. USAE response spectrum (top) and summed USAE amplitude (bottom) over small frequency range during heating/cooling in fresh porcine muscle *ex vivo*.

The results of nine porcine muscle samples and nine porcine fat samples are normalized and plotted against temperature in

Figure 4-14 below. These results were obtained during the heating portion of temperature scans in fresh porcine tissue like those previously described. The fat

measurements were made using an acoustical power of 10.6 W per USAE pulse, while the muscle scan used 17.2 W per USAE pulse. For each scan, the data is normalized by the initial USAE value which was calculated by averaging the USAE response over ten initial pulses taken at the baseline temperature. The USAE values at each temperature are averaged over all nine samples and a standard error is calculated. The relationship is appears to be linear up to about 50°C. The change in the slope at this temperature may be a result of tissue coagulation at higher temperatures.
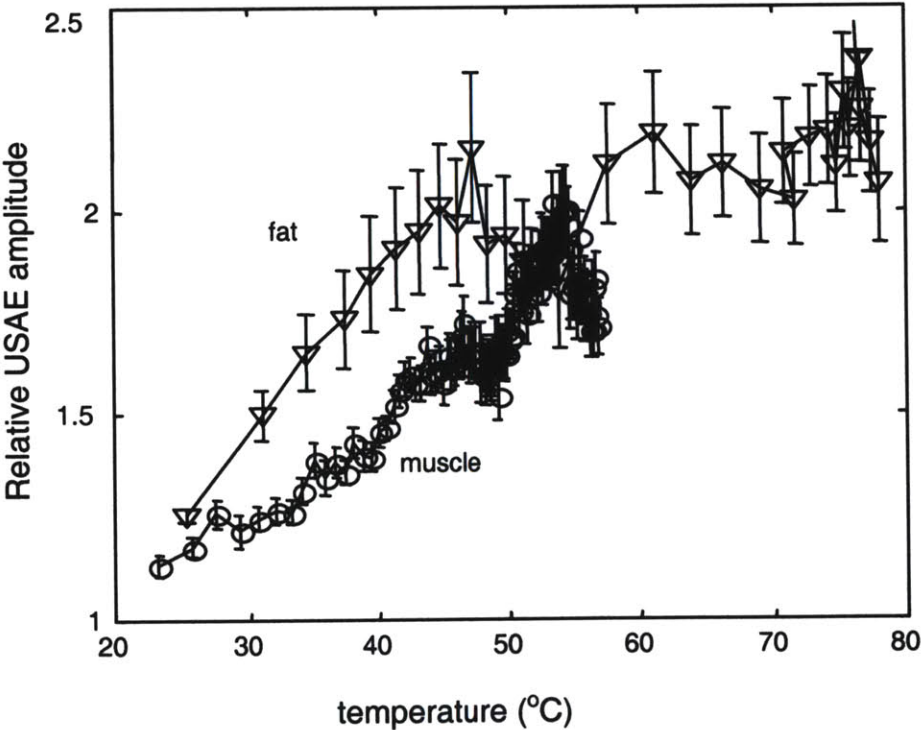
Figure 4-14. The relative USAE amplitude at increasing temperatures during heating of porcine muscle and porcine fat. Normalized amplitude averaged over nine samples with standard error is plotted.

4.2.4 *Cavitation*

Although the USAE amplitudes tended to follow the sample temperature fairly well at lower powers, the temperature scan results did not always demonstrate a smooth increase and decrease in USAE amplitude with rising and falling temperatures. In many cases, the amplitudes fluctuated wildly and randomly. These cases occurred exclusively at higher USAE amplitude pulses and offer intriguing support for using this method to detect cavitation.

Cavitation refers to the formation of bubbles during the application of ultrasound energy due to the fluctuating high intensity pressure field. Cavitation during thermal surgery often results in drastic temperature fluctuations and tissue damage. Tiny bubbles form and implode, causing shock waves and non-linear effects in the tissue. However, researchers may be able to use this phenomenon to facilitate HIFU surgery. Currently, cavitation is detected by the broadband pulse of energy released by the imploding bubbles.

The USAE method may be an effective way to detect cavitation in tissues. Support for this application is based on empirical results from scans in fresh porcine muscle and fat using the chirp technique. During some of the higher power experiments, a chirping sound was heard coming from the tank. These sounds were noted for each experiment during which they occurred. The following four characteristics from empirical data and observation serve as evidence for the detection of cavitation during a USAE scan.

First, the cavitating scan is accompanied by an irregular temperature profile during heating, while the non-cavitating scan demonstrates a characteristically smooth

70

exponential temperature rise. The literature describes this effect of cavitation on the heating profile of tissue [22]. It is due to both bubble shielding which would cause temperatures to decrease abruptly and bubble implosion which would cause sudden spikes in pressure and temperature.

Second, the cavitating scan has a rapidly fluctuating USAE amplitude while the non-cavitating scan has a smooth response. Although the non-cavitating scan does not always show a perfect correlation between USAE amplitude and temperature, it tends to rise and fall with temperature. If it does not follow temperature well but is erratic, the fluctuations occur in heating and cooling parts of the scan and are never more than 100% of the average USAE amplitude. In contrast, during cavitating scans, there are sudden drops in USAE amplitude even while the tissue is still heating. The USAE amplitude fluctuations are sometimes as large as 1000% or more and occur primarily during the heating phase because this is the portion of the scan during which large energies are deposited into the tissue which may aid in bubble formation and collapsing. The large amplitudes may be associated with spikes in temperature, but are more likely due to reflection from gas bubbles since the temperatures do not fluctuate enough to explain the enormous fluctuations in USAE response. In addition, the USAE amplitude is very sensitive to fluctuations in the radiation force which is affected by the presence of gas bubbles.

Third, the response wave of the cavitating scan is a broadband response across all frequencies, including those not sent in the chirp pulse, while the response of the non-cavitating scan shows a very distinct cut-off at the frequencies sent in the chirp pulse. This is one of the most convincing observations about cavitating scans because the

broadband response during cavitation is well documented in the literature [22]. In our case, the diagnostic USAE chirp pulse sent to the sample contains frequencies from 1 kHz to 20 kHz. In those scans that are not categorized as having cavitated, the FFT of the response shows a sharp cut-off below 1 kHz and above 20 kHz. In cavitating scans, the FFT of the response shows a large contribution to the signal across all frequencies from 0 kHz to 25 kHz (where 25 kHz is the limit of the FFT based on the sample rate of the measuring equipment).

Fourth, the cavitating scan makes an audible 'chirping' sound, while the non-cavitating scan makes no audible sound. While the exact nature of this peculiar sound is not clear, it is probably related to the enormous amplitudes of the USAE response in the cavitating scans. Trapped gas from cavitation may create an impedance mismatch in the tissue which leads to a large radiation force and the resulting USAE response. This response is so large in the cavitation cases, that it is audible to the unaided ear in the vicinity of the experimental tank. The 'chirping' sound was noted for each scan during which it was observed. After subsequent data analysis, this sound was correlated exclusively with scans that demonstrated the other three characteristics of cavitation.

In addition, the fluctuating temperatures, fluctuating USAE amplitudes, broadband response, and chirping sounds were observed almost exclusively in scans at higher power levels (10.6 W and higher). This further supports the cavitation theory because cavitation is more likely to occur at higher power levels.

The following two scans have been classified as non-cavitating (Figure 4-15) and cavitating (Figure 4-16) based on the four criteria, and serve as a representative sample of the scans performed in fresh tissue. Almost every one of the hundreds of scans

performed can be categorized as either having cavitated or not cavitated based on the four factors. Notice the broadband frequency response of the cavitating sample (Figure 4-16) which occurs from t=20 sec to t=80 sec during the heating phase of the scan. This is the portion during which cavitation occurred. Cavitation is also evident from the erratic temperature profile during this time period and the erratic USAE amplitude response.
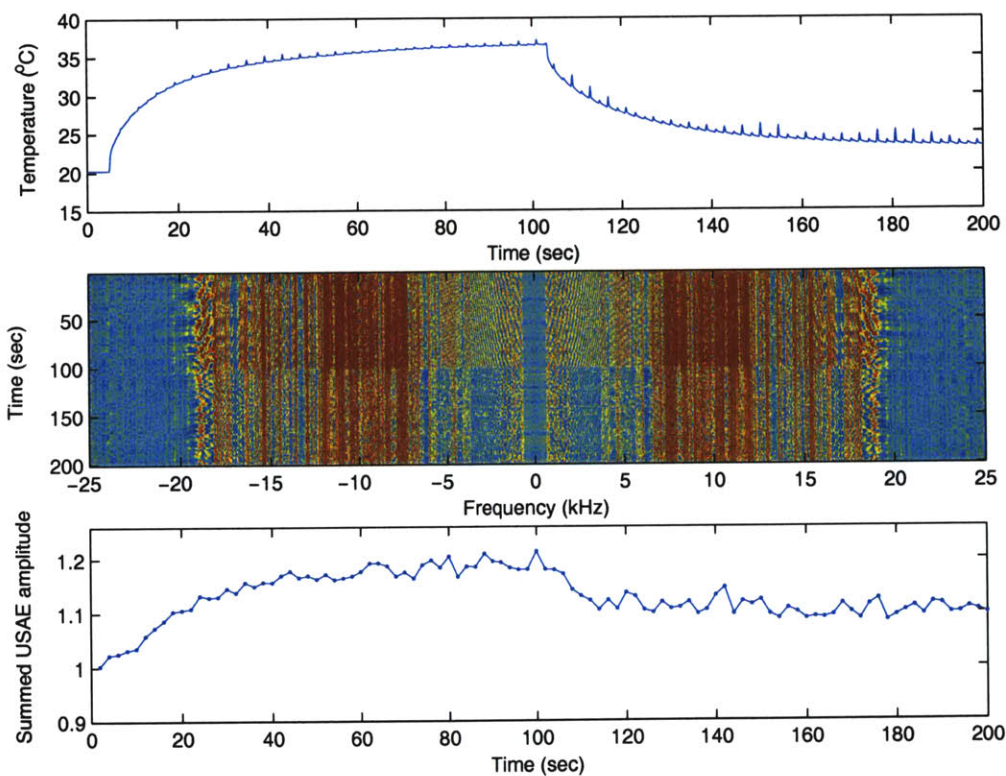
Figure 4-15. Example of summed USAE amplitude (top), USAE response spectrum (middle), and temperature (bottom) during heating/cooling of fresh porcine fat without the presence of cavitation. USAE pulses at 6.6 W acoustical power.
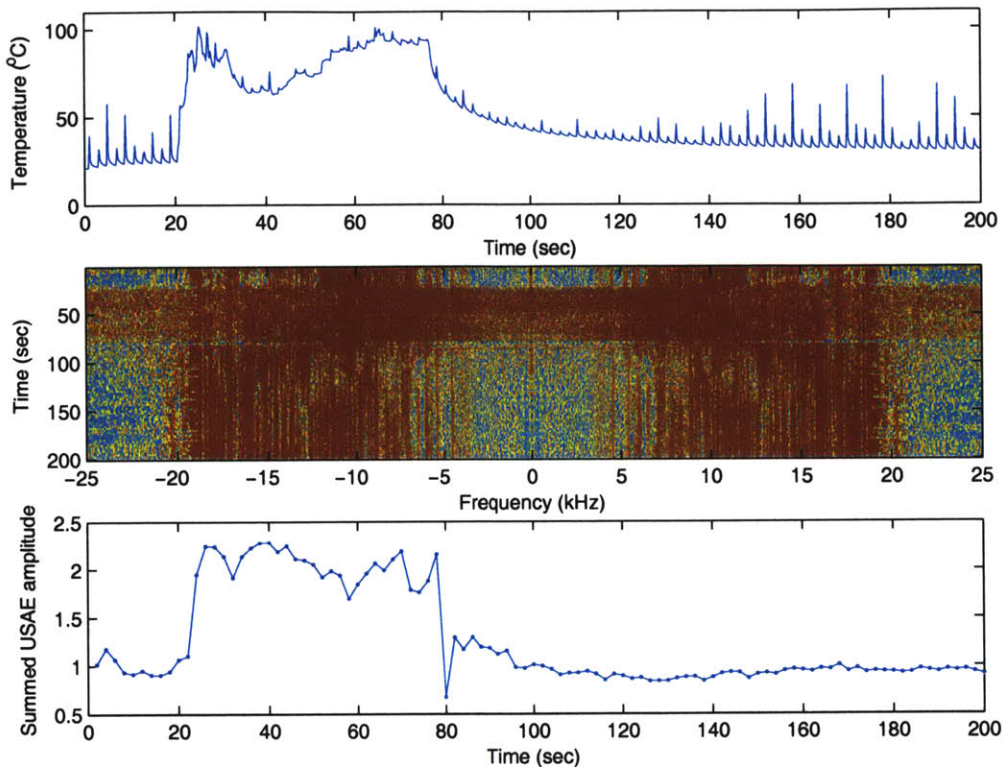
Figure 4-16. Example of summed USAE amplitude (top), USAE response spectrum (middle), and temperature (bottom) during heating/cooling of fresh porcine fat with the presence of cavitation. USAE pulses at 17.2 W acoustical power.

5   Discussion

The USAE method is a promising new means for monitoring and controlling thermal surgery. The simplified mechanical model and finite element simulations along with the experimental results demonstrate the complex interdependence of the sample temperature, stiffness, acoustic absorption coefficient, gas bubble content and the amplitude of the USAE response. The high sensitivity of the USAE response to

variations in the tissues scanned and experimental conditions made it difficult to repeat scans in a manner which would allow for direct comparison between scans of different tissues on different days. Certain tissue cavitated when pulsed at 10.6 W, while others did not. Some tissues cavitated at temperatures near 100°C, while others cavitated at temperatures closer to 60°C. Additionally, some tissues heated very quickly while others did not.

Despite these biological and experimental variations, the experimental results provide insight into the USAE response and the properties that influence its amplitude. The frequency scans at a single difference frequency did not usually show the same response spectrum for different samples scanned. However, they usually showed an increase in the USAE amplitude at certain frequencies after having necrosed the tissue. Although these optimal frequencies which showed the greatest increase in amplitude varied among samples, they most often occurred at the peaks of the spectrum taken before the tissue was necrosed.

One explanation for this finding is that the spectrum of the response is affected both by the tissue's true response spectrum and the transfer functions of the various equipment involved in acquiring the signal. Although it may be true that the tissue absorbs and subsequently emits more acoustical energy at certain frequencies, the mechanical and electrical systems are not perfect transducers of the response signal either. Perhaps the spikes exist at the frequencies at which the signal from the tissue is most amplified by the physical set-up like the tank dimensions and the electrical components, like the hydrophone and pre-amplifier. One piece of evidence that supports the hypothesis that the transfer function of the set-up may affect the response spectrum is

that the spectrum was spiked at certain frequencies (e.g. 7 kHz) for many different sample types. Regardless of the source of amplification at certain frequencies, this amplification would tend to exaggerate the difference between the pre- and post-necrosis USAE amplitudes. Therefore, the largest difference between the pre- and pos-necrosis USAE amplitudes would exist at the spikes in the pre-necrosis scan spectrum.

Another explanation for the fact that the greatest change in the USAE response amplitude occurred at the spikes of the pre-necrosis response spectrum is related to cavitation. Although the frequency scans and chirp scans were performed at power levels that would not normally produce cavitation events in the tissue, after the tissue is necrosed, the cavitation threshold may decrease. Therefore, the scans conducted after necrosis of the tissue may have a higher probability of cavitating during the USAE pulse. Further, the post-necrosis scans would show the greatest USAE amplitude changes at the spikes on the pre-necrosis spectrum if these spikes represent the frequencies at which the tissue has a higher acoustic absorption coefficient because cavitation would be more likely at these frequencies. Evidence to support this explanation include the fact that the audible single difference frequency described in the cavitation section above was also sometimes heard during frequency scans after necrosis.

In addition to the frequency scans described above, the scans performed with a single chirp pulse before and after creating a lesion revealed similar results. In the example of a chirp scan presented above (Figure 4-8), the amplitudes at almost all frequencies were larger after the lesion was formed. Note that the spectrum of the pre-necrosis pulse is similar to that of the frequency scan depicted in

Figure 4-1 because they both have a large spike at 10.2 kHz and 12 kHz. Another similarity between the single frequency and chirp scans is that in some scans no clear difference in USAE amplitude was observed before and after the lesion was formed. One plausible explanation for this inconsistency between experiments is the decreased cavitation threshold of the necrosed tissue and the resulting unpredictability of a cavitation event occurring. Another explanation is the complex change in both absorption and stiffness which have counteractive effects. In some cases, they may balance one another and produce no net change in USAE amplitude.

Ultimately, the USAE method appears to be effective in detecting necrosed tissue. However, it is still not clear if the tissue response is affected by the necrosis itself or by cavitation events (which will almost always result in tissue necrosis). Although the possibility of cavitation was raised by the difficulty in reproducing these necrosis detection experiments, there is one very good piece of evidence against the cavitation explanation of increased USAE amplitude after necrosis. Assuming that four cavitation characteristics described above in the results section are predictive of cavitation events, then the line scan performed with the chirp technique (Figure 4-9) would refute the cavitation explanation of increased USAE amplitude after necrosis. In this experiment, the necrosed tissue is clearly distinguishable from the healthy tissue while the image of the chirp response reveals no broadband response from the necrosed tissue. The response stops abruptly at the highest difference frequency of the chirp pulse (20 kHz) rather than demonstrating a uniform response throughout the frequencies of the FFT as is indicative of a cavitating event according to the analysis presented in this thesis. In addition, no audible 'chirping' was detected during this line scan. Cavitation may explain some cases

of increased USAE amplitude after necrosis, but there is at least one definitive result which shows an increased USAE amplitude after necrosis without demonstrating any characteristics of cavitation events.

The line and area scans used to detect necrosed tissue are simply a 2-D extension of the single location scans. They offered an advantage over the single location scans in that there were many more data points acquired over the entire scan. Because of the large amount of data, the images of necrosed tissue were perceptible to the eye despite the low USAE amplitudes at many locations within the necrosed region because on average, the amplitude of the response was much larger within the region of the necrosed tissue than in healthy tissue. The only problem with line and area scans is that the time period over which they were performed often spanned an hour or more. This time frame could be substantially reduced by: 1) decreasing the duration of the pause between the pulses, 2) stepping the transducer more quickly via a faster mechanical system, or 3) electronically steering the focus using phasing techniques with a multi-element array. The line and area scans offer powerful evidence that this system can be used to effectively image regions of tissue during thermal surgery.

Temperature experiments were all performed using the chirp technique. Similar to the necrosis experiments, the temperature experiments did not always reveal smooth exponential USAE amplitude curves. This is partially due to cavitation at higher power levels and poor signal-to-noise ratio at lower power levels. The experiment in which five lesions were scanned at five different power levels in rabbit liver (Figure 4-3) illustrates the effect of power level on USAE response. Although the USAE amplitude does not depend exclusively on temperature, the strong relationship between temperature and

absorption in the range of heating before tissues begin to develop necrosis undoubtedly affects the USAE signal for medium power heating experiments. The USAE amplitude summed over all frequencies was temperature-dependant in most experiments. In every experiment there were optimal frequency ranges that followed the temperature even more closely than the total summed amplitude. The summed USAE amplitude method is desirable to create a frequency-independent method to monitor temperature (due to the uncertainty regarding which frequencies will respond the best to temperature changes). It may be possible to develop a more accurate method for determining the best frequencies to use. One possibility is a computer algorithm that would search all frequencies and find a least squared error between the USAE amplitude and the temperature. This method assumes that temperature directly affects USAE amplitude in a linear fashion. There are other possibilities for refining the system such that an optimal frequency is determined based on the results of a chirp scan.

Many of the temperature experiments which used high powers exhibited audible chirp sounds, a characteristic broadband response, and erratic temperature and summed USAE amplitude response. The strong correlation between these four factors and cavitation makes the USAE method a promising predictor of cavitation.

6   Conclusions

Fatemi and Greenleaf first proposed the USAE method in an article in *Science* in 1998 as a new method of non-destructive testing. Until now, the only published experimental results (besides those of the author and collaborators at FUS Laboratory)

have involved imaging tuning forks and calcified plaques, both very stiff and dense materials. This thesis presents the broad application of the USAE method for monitoring various aspects of thermal surgery.

The USAE method shows promise in detecting necrosis, temperature elevations, and cavitation in biological tissues. The USAE experiments presented in this thesis demonstrate the ability to sense temperature elevations before necrosis occurs which is an important first step in positioning a FUS system without the need for MRI guidance. In addition, the experiments demonstrate the feasibility of imaging necrosed tissue and detecting cavitation. Both capabilities will aid in monitoring thermal surgery. It may also be possible to calibrate the USAE response so that it yields an exact temperature measurement. The USAE method may prove useful as an entirely new imaging modality to aid in thermal surgery and beyond because it can potentially image the mechanical properties of tissue. Further refinement of the system is necessary and additional experiments for statistical significance of the measurements are essential. Still, the images of necrosis, temperature plots, and cavitation spectral plots rendered with the USAE method are compelling.

Future experiments will utilize a new amplifier system, custom-built for use with the USAE system. This amplifier has built-in function generators and power feedback control to ensure more even pulse amplitudes and lower system noise. Also, a new hydrophone will be used that offers greater sensitivity and broader frequency response making it possible to explore higher frequencies. The next step includes *in vivo* experimentation, which should offer several advantages over the *ex vivo* experiments. For example, the greatly increased cavitation threshold in a living animal will likely

reduce cavitation-induced instability and will allow for a larger signal-to-noise ratio since the USAE pulse amplitude can be increased without inducing cavitation. A living animal more closely represents the environment in which a diagnostic USAE system will need to operate.

The USAE method is a simple but clever acoustical idea of combining slightly differing high frequency fields to produce a low frequency beat signal at the focal point which can be used to locally stimulate an object. The possibilities of this method of remote excitation are vast. In this preliminary exploration of the uses and applications of the USAE method as applied to medical imaging, a wealth of information regarding the interaction of tissues and the USAE signal was discovered. The complexity of the acoustical and mechanical problems involved in extracting useful information from the USAE response signal makes this research rich with possibilities for applications and intellectual pursuit.

7 Appendix A: Transducer Characterization

7.1 Left/Right Transducer
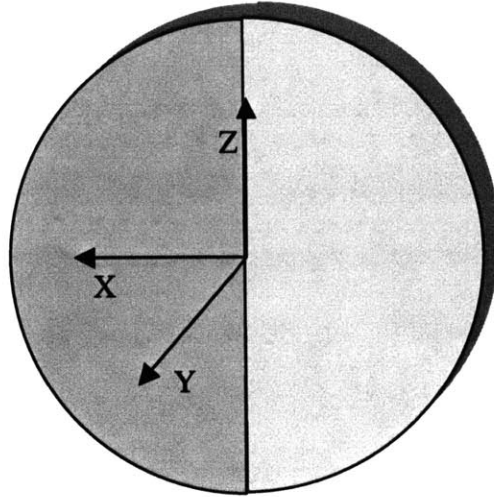
Figure 7-1. Diagram of left/right element array.

7.1.1 Efficiencies

7.1.1.1 Left Element

Electric Input (VPP)	Average Electric Power (W)	Average Acoustic Power (W)	Standard Error of Measurement	Efficiency (%)
0.03	2.54E-01	1.70E-01	2.42E-03	67.06
0.05	6.85E-01	4.47E-01	5.04E-03	65.31
0.07	1.33E+00	8.91E-01	6.89E-03	67.03
0.09	2.17E+00	1.45E+00	9.35E-03	66.84
0.11	3.23E+00	2.16E+00	1.08E-03	66.87
0.13	4.54E+00	3.05E+00	1.81E-02	67.14
0.15	6.03E+00	4.05E+00	1.10E-02	67.14
0.17	7.76E+00	5.21E+00	1.99E-02	67.16
0.19	9.70E+00	6.49E+00	2.00E-02	66.9
0.21	1.19E+01	7.95E+00	1.49E-02	66.96
0.23	1.42E+01	9.56E+00	1.59E-02	67.35
0.25	1.68E+01	1.13E+01	1.24E-02	67.05
0.27	1.96E+01	1.31E+01	4.28E-02	66.9
0.29	2.27E+01	1.51E+01	2.75E-02	66.61

Table 7-1. Efficiencies at various powers for left element of left/right element array.

7.1.1.2 Right Element

Electric Input (VPP)	Average Electric Power (W)	Average Acoustic Power (W)	Standard Error of Measurement	Efficiency (%)
0.03	2.53E-01	1.65E-01	4.48E-03	65.35
0.05	7.00E-01	4.45E-01	5.18E-03	63.6
0.07	1.37E+00	8.82E-01	5.49E-03	64.42
0.09	2.25E+00	1.45E+00	6.46E-03	64.66
0.11	3.36E+00	2.18E+00	1.44E-03	64.97
0.13	4.69E+00	3.03E+00	7.56E-03	64.67
0.15	6.24E+00	4.05E+00	2.42E-02	64.89
0.17	8.02E+00	5.18E+00	1.88E-02	64.5
0.19	1.00E+01	6.51E+00	9.34E-03	64.89
0.21	1.23E+01	7.94E+00	8.48E-03	64.56
0.23	1.47E+01	9.46E+00	8.56E-02	64.35
0.25	1.74E+01	1.12E+01	2.94E-02	64.56
0.27	2.03E+01	1.31E+01	6.85E-03	64.56
0.29	2.34E+01	1.51E+01	4.14E-02	64.43

Table 7-2. Efficiencies at various powers for right element of left/right element array.

7.1.2 Pressure Fields
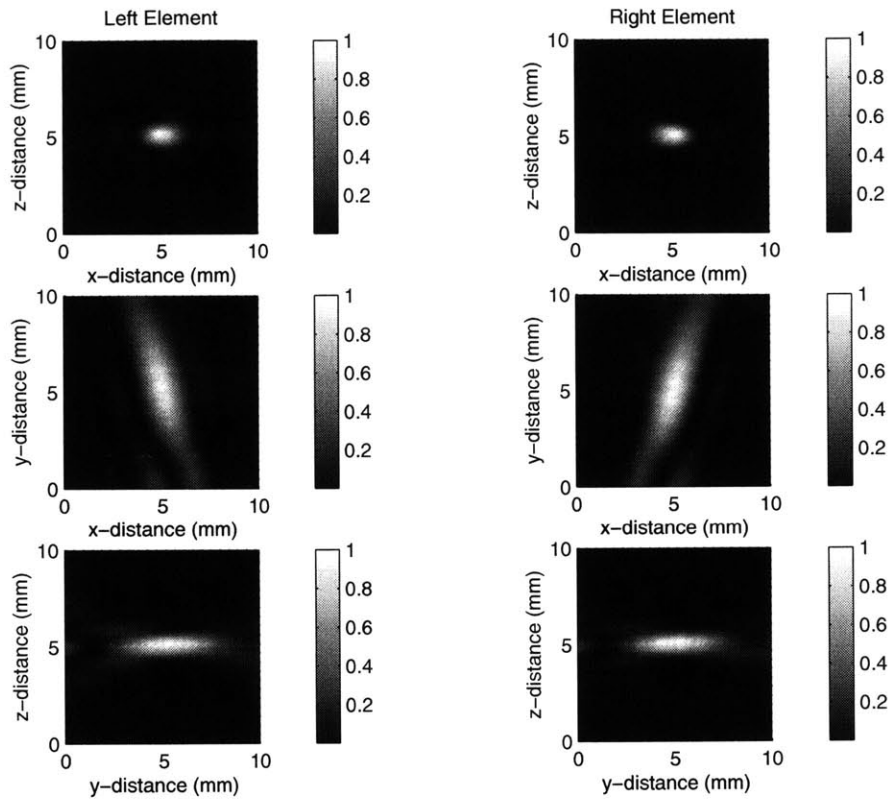
Figure 7-2. Normalized pressure fields of left element (left column) and right element (right column) of left/right element array in XZ, XY, and YZ planes through focus.

7.2 Co-axial Transducer

Figure 7-3. Diagram of inner/outer elements of co-axial array.

7.2.1 Efficiencies

7.2.1.1 Inner Ring Element

Electric Input (VPP)	Average Electric Power (W)	Average Acoustic Power (W)	Standard Error of Measurement	Efficiency (%)
0.03	2.49E-01	1.96E-01	2.63E-03	78.84
0.05	6.88E-01	5.51E-01	3.46E-03	80.07
0.07	1.34E+00	1.07E+00	2.88E-03	79.97
0.09	2.18E+00	1.74E+00	2.36E-03	79.94
0.11	3.25E+00	2.61E+00	1.03E-02	80.17
0.13	4.56E+00	3.66E+00	1.21E-02	80.25
0.15	6.06E+00	4.84E+00	1.33E-02	79.95
0.17	7.80E+00	6.25E+00	1.45E-02	80.13
0.19	9.74E+00	7.80E+00	1.99E-02	80.03
0.21	1.19E+01	9.55E+00	3.95E-02	80.12
0.23	1.43E+01	1.14E+01	2.31E-02	79.93
0.25	1.69E+01	1.35E+01	7.82E-03	80.04
0.27	1.97E+01	1.58E+01	8.27E-03	80.03
0.29	2.28E+01	1.82E+01	2.99E-02	79.68

Table 7-3. Efficiencies at various powers for inner element of co-axial array.

7.2.1.2 Outer Ring Element

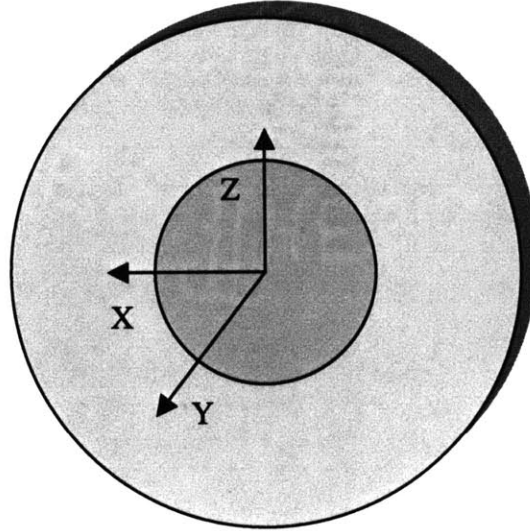| Electric Input (VPP)	Average Electric Power (W)	Average Acoustic Power (W)	Standard Error of Measurement	Efficiency (%)
0.03	2.41E-01	1.58E-01	8.78E-03	65.7
0.05	6.63E-01	4.21E-01	3.25E-03	63.41
0.07	1.30E+00	8.28E-01	1.24E-03	63.91
0.09	2.13E+00	1.37E+00	4.19E-03	64.15
0.11	3.18E+00	2.06E+00	1.86E-03	64.63
0.13	4.44E+00	2.86E+00	8.80E-03	64.46
0.15	5.90E+00	3.77E+00	3.13E-02	63.92
0.17	7.59E+00	4.90E+00	2.11E-02	64.56
0.19	9.50E+00	6.16E+00	1.26E-02	64.79
0.21	1.16E+01	7.48E+00	1.46E-02	64.34
0.23	1.39E+01	8.97E+00	3.98E-02	64.49
0.25	1.65E+01	1.06E+01	7.31E-03	64.48
0.27	1.92E+01	1.24E+01	1.93E-02	64.61
0.29	2.22E+01	1.43E+01	1.72E-02	64.42

Table 7-4. Efficiencies at various powers for outer element of co-axial array.

7.2.2   *Pressure Fields*
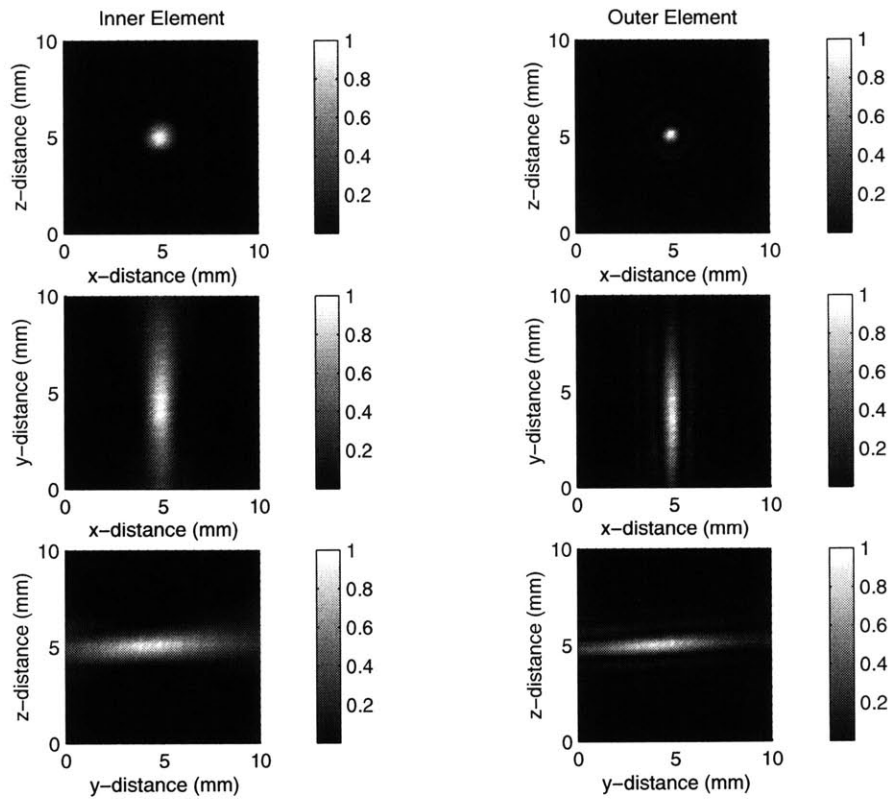
Figure 7-4. Normalized pressure fields of inner element (left column) and outer element (right column) of co-axial array in XZ, XY, and YZ planes through focus.

Reference List

[1] B.E. Billard, K. Hynynen, and R.B. Roemer, Effects of physical parameters on high temperature ultrasound hyperthermia *Ultrasound Med.Biol.*, vol. 16, pp. 409-420, 1985.

[2] A.K. Burov, High intensity ultrasonic oscillations for the treatment of malignant tumors in animal and man *Dokl Akad Nauk SSSR*, vol. 106, pp. 239-241, 1956.

[3] A.K. Burov and G.D. Adreevskaya, The effect of ultra-acoustic oscillation of high intensity on malignant tumors in animals and man *Dokl Akad Nauk SSSR*, vol. 106, pp. 445-448, 1956.

[4] N.L. Bush, I. Rivens, G.R. ter Haar, and J.C. Bamber, Acoustic properties of lesions generated with an ultrasound therapy system *Ultrasound Med.Biol.*, vol. 19, pp. 789-801, 1993.

[5] I. Cespedes, J. Ophir, H. Ponnekanti, and N. Maklad, Elastography: elasticity imaging using ultrasound with application to muscle and breast in vivo *Ultrason.Imaging*, vol. 15, pp. 88, 1993.

[6] L. Chen, H.G. tar, C.R. Hill, S.A. Eccles, and G. Box, Treatment of implanted liver tumors with focused ultrasound, *Ultrasound Med.Biol.*, vol. 24, pp. 1475-1488, Nov. 1998.

[7] L. Crum and K. Hynynen, Sound therapy *Phys.World (UK.)*, vol. 9, no. 8, pp. 28 1996. 0953-8585.

[8] C.A. Damianou, N.T. Sanghvi, and F.J. Fry, Ultrasonic attenuation of dog tissues as a function of temperature *1995 IEEE Ultrasonics Symposium. Proceedings. An International Symposium (Cat.No.95CH35844.)*, vol. pp. 1203, 1995.

[9] M.M. Doyley, J.C. Bamber, I. Rivens, N.L. Bush, and G.R. ter Haar, Elastographic imaging of thermally ablated tissue in vitro, IEEE-UFFC Symp. AnonymousAnonymous1999. Lake Tahoe, NV.

[10] X. Fan and K. Hynynen, Ultrasound surgery using multiple sonications - treatment time considerations *Ultrasound Med.Biol.(USA)*, vol. 22, pp. 471-482, 1996.

[11] M. Fatemi and J.F. Greenleaf, Ultrasound-stimulated vibro-acoustic spectrography *Science*, vol. 280, pp. 82-85, Apr. 3, 1998.

[12] M. Fatemi and J.F. Greenleaf, Application of radiation force in noncontact measurement of the elastic parameters *Ultrason.Imaging*, vol. 21, pp. 147-154, Apr. 1999.

[13] M. Fatemi and J.F. Greenleaf, Vibro-acoustography: An imaging modality based on ultrasound-stimulated acoustic emission *Proc.Natl.Acad.Sci.U.S.A.*, vol. 96, pp. 6603-6608, Jun 8. 1999.

[14] L.A. Frizzell, C.A. Linke, E.L. Carstensen, and C.W. Fridd, Thresholds for focal ultrasonic lesions in rabbit kidney, liver and testicle *IEEE Trans.Biomed.Eng.(USA)*, vol. BME-24, pp. 393-396, 1977.

[15] F.J. Fry, Intense focused ultrasound in medicine. Some practical guiding physical principles from sound source to focal site in tissue *Eur.Urol.*, vol. 23 Suppl 1, pp. 2-7, 1993.

[16] F.J. Fry and L.K. Johnson, Tumor irradiation with intense ultrasound *Ultrasound.Med.Biol.*, vol. 4, pp. 337-341, 1978.

[17] F.J. Fry and L.K. Johnson, Tumor irradiation with intense ultrasound *Ultrasound Med.Biol.(USA)*, vol. 4, pp. 337-411, 1978.

[18] B.S. Garra, I. Cespedes, J. Ophir, R.S. Spratt, R.A. Zuurbier, C.M. Magnant, and M.F. Pennanen, Elastography of breast lesions: Initial clinical results *Radiology*, vol. 202, pp. 86, 1997.

[19] J. Horvath, Ultraschallwirkung beim menshlichen sarkom *Strahlentherapie*, vol. 75, pp. 1191944.

[20] K. Hynynen. Biophysics and Technology of Ultrasound Hyperthermia., 1990, pp. 61-115.

[21] K. Hynynen, Demonstration of enhanced temperature elevation due to nonlinear propagation of focussed ultrasound in dog's thigh in vivo *Ultrasound Med.Biol.*, vol. 13, pp. 85-91, Feb. 1987.

[22] K. Hynynen, The threshold for thermally significant cavitation in dog's thigh muscle in vivo *Ultrasound Med.Biol.*, vol. 17, pp. 157-169, 1991.

[23] K. Hynynen, Focused ultrasound surgery guided by MRI *Science&Medicine*, vol. 3, pp. 62-71, 1996.

[24] K. Hynynen, A. Chung, T. Fjield, M. Buchanan, D. Daum, V. Colucci, P. Lopath, and F.A. Jolesz, Feasibility of using ultrasound phased arrays for MRI monitored noninvasive surgery *IEEE Trans. Ultrason. Ferroelectr. Freq. Control (USA)*, vol. 43, no. 6, pp. 1043 1996. 0885-3010.

[25] K. Hynynen, A. Darkazanli, E. Unger, and J.F. Schenck, MRI-guided
      noninvasive ultrasound surgery *Med.Phys.*, vol. 20, pp. 107-115, Jan.
      1993.

[26] Y. Ishihara, A. Calderon, H. Watanabe, K. Okamoto, Y. Suzuki, and K. Kuroda,
      A precise and fast temperature mapping using water proton chemical shift
      Magn.Reson.Med., vol. 34, pp. 814-823, Dec. 1995.

[27] J.W. Jenne, M. Bahner, J. Spoo, P. Huber, R. Rastert, I. Simiantonakis, W.J.
      Lorenz, and J. Debus, CT on-line monitoring of HIFU therapy *1997
      IEEE Ultrasonics Symposium Proceedings.An International Symposium
      (Cat.No.97CH36118.)*, vol. pp. 1377, 1997.

[28] C. Johnson, Nonionizing electromagnetic wave effects in biological materials and
      system *Proc of the IEEE*, vol. 60, pp. 692-718, 1972.

[29] F. Kallel, R.J. Stafford, R.E. Price, R. Righetti, J. Ophir, and J.D. Hazle, The
      feasibility of elastographic visualization of HIFU-induced thermal lesions
      in soft tissues. Image-guided high-intensity focused ultrasound
      Ultrasound Med.Biol., vol. 25, pp. 641-647, May. 1999.

[30] T. Karjalainen, J.S. Thierman, and K. Hynynen, Ultrasound Stimulated Acoustic
      Emission for Controlling Thermal Surgery, IEEE-UFFC Symp., pp. 1397-
      1400, 1999. Lake Tahoe, NV.

[31] E.E. Konofagou and J. Ophir, A new elastographic method for estimation and
      imaging of lateral strains, corrected axial strains and poison's ratios in
      tissues *Ultrasound Med.Biol.(USA)*, vol. 24, pp. 1183-1199, 1998.

[32] E.E. Konofagou, J.S. Thierman, and K. Hynynan, A Focused Ultrasound Method
      for Synchronous Diagnostic and Therapeutic Applications – A Simulation
      Study *Phys Med.Biol.* [in process], vol. 2000.

[33] T.A. Krouskop, T.M. Wheeler, F. Kallel, B.S. Garra, and T. Hall, The elastic
      moduli of breast and prostate tissues under compression
      Ultrason.Imaging, vol. 20, pp. 260-274, 1998.

[34] P.P. Lele, Production of deep focal lesions by focused ultrasound - current status
      Ultrasonics, vol. 5, pp. 105-122, 1967.

[35] P.P. Lele, Hyperthermia by ultrasound, pp. 168-178, 1975. Proceedings of the
      international symposium on cancer therapy by hyperthermia and
      radiation., Washington.

[36] P.P. Lele, Threshold and mechanisms of ultrasonic damage to organized animal
      tissues *Proceedings of a Symposium on Biological effects and*

characterization of ultrasound sources, vol. Rockville, MA, no. June 1-3, pp. 224-239, 1977.

[37] N.J. McDannold, K. Hynynen, D. Wolf, G. Wolf, and F.A. Jolesz, MRI evaluation of thermal ablation of tumors with focused ultrasound *J.Magn.Reson.Imaging*, vol. 8, pp. 91-100, Jan. 1998.

[38] R. Muthupullai, P.J. Rossman, D.J. Lomas, J.F. Greenleaf, and R.L. Ehman, Magnetic resonance elastography *Science*, vol. 269, pp. 1854-1857, 1995.

[39] K. Nightingale, R. Nightingale, M. Palmeri, and G. Trahey, Finite-element analysis of radiation force induced tissue motion with experimental validation, IEEE-UFFC Symp., pp. 1319-1322, 1999. Lake Tahoe, NV.

[40] M. Oka, Surgical application of high-intensity focused ultrasound *Clin All Round(Jpn)*, vol. 13, pp. 1514, 1960.

[41] J. Ophir, I. Cespedes, H. Ponnekanti, Y. Yazdi, and X. Li, Elastography: a quantitative method for imaging the elasticity of biological tissues *Ultrason.Imaging*, vol. 13, pp. 111-134, 1991.

[42] K.J. Parker, S.R. Huang, R.A. Musulin, and R.M. Lerner, Tissue response to mechanical vibrations for sonoelasticity imaging *Ultrasound Med.Biol.*, vol. 16, pp. 241-246, 1990.

[43] F. Prat, M. Centarti, A. Sibille, A. Fadil, L. Henry, J.Y. Chapelon, and D. Cathignol, Extracorporeal high-intensity focused ultrasound for VX2 liver tumors in the rabbit *Hepatology*, vol. 21, pp. 832-836, 1995.

[44] F. Prat, J.Y. Chapelon, A. Fadil, A. Sibille, Y. Theilliere, T. Ponchon, and D. Cathignol, Focused liver ablation by cavitation in the rabbit: a potential new method of extracorporeal treatment *Gut*, vol. 35, pp. 395-400, Mar. 1994.

[45] S.S. Rao, Mechanical Vibrations, 3rd edition, 1995. Addison-Wessley. Reading, MA.

[46] M. Ribault, J.Y. Chapelon, D. Cathignol, and A. Gelet, Differential attenuation imaging for the characterization of high intensity focused ultrasound lesions *Ultrason.Imaging*, vol. 20, pp. 160-177, Jul. 1998.

[47] R. Righetti, F. Kallel, R.J. Stafford, R.E. Price, T.A. Krouskop, J.D. Hazle, and J. Ophir, Elastographic characterization of HIFU-induced lesions in canine livers *Ultrasound Med.Biol.*, vol. 25, pp. 1099-1113, Sep. 1999.

[48] N.T. Sanghvi, Role of cavitation during high intensity focused ultrasound treatment of prostate tissue AnonymousAnonymouspp. 1067-1068, 1998. Proceedings 16th International Congress on Acoustics and the 135th Meeting of the Acoustic Society of America.

[49] N.T. Sanghvi, F.J. Fry, R. Bihrle, R.S. Foster, M.H. Phillips, J. Syrus, A.V. Zaitsev, and C.W. Hennige, Noninvasive surgery of prostate tissue by high-intensity focused ultrasound *IEEE Trans. Ultrason. Ferroelectr. Freq. Control (USA)*, vol. 43, no. 6, pp. 1099, 1996.

[50] X. Shi, R.W. Martin, D. Rouseff, S. Vaezy, and L.A. Crum, Detection of high-intensity focused ultrasound liver lesions using dynamic elastometry *Ultrason.Imaging*, vol. 21, pp. 107-126, Apr. 1999.

[51] R.J. Stafford, F. Kallel, R.E. Price, D.M. Cromeens, T.A. Krouskop, J.D. Hazle, and J. Ophir, Elastographic imaging of thermal lesions in soft tissue: a preliminary study in vitro, *Ultrasound Med.Biol.*, vol. 24, pp. 1449-1458, Nov. 1998.

[52] T. Sugimoto, S. Ueha, and K. Itoh, Tissue hardness measurement using the radiation force of focused ultrasound, 1990 IEEE Ultrasonics Symposium Proceedings, pp. 1377-1380, 1990.

[53] A. Szent-Gorgyi, Chemical and biological effects of ultrasonic radiation *Nature*, vol. 131, pp. 278, 1933.

[54] G. ter Haar, Ultrasound focal beam surgery *Ultrasound Med.Biol.*, vol. 21, pp. 1089-1100, 1995.

[55] G. ter Haar, D. Sinnett, and I. Rivens, High intensity focused ultrasound--a surgical technique for the treatment of discrete liver tumours *Phys.Med.Biol.*, vol. 34, pp. 1743-1750, Nov, 1989.

[56] G. Torr, The acoustic radiation force *Am.J.Phys.*, vol. 52, pp. 402-408, 1984.

[57] G. Vallancien, E. Chartier-Kastler, N. Bataille, D. Chopin, M. Harouni, and J. Bougaran, Focused extracorporeal pyrotherapy *Eur.Urol.*, vol. 23, pp. 48-52, 1993.

[58] F.S.M. Van Kleef, J.V. Bosqamp, and M. Van Den Tempel, Determination of the Number of Cross-Links in a Protein Gel from its Mechanical and Swelling Properties *Biopolymers*, vol. 17, pp. 225-235, 1978.

[59] P. VanBaren, J.-U. Kluiwstra, R. Seip, Y. Zhang, E.S. Ebbini, and C.A. Cain, 2D large aperture ultrasound phased arrays for hyperthermia cancer therapy: design, fabrication and experimental results *1995 IEEE Ultrasonics*

Symposium.Proceedings.An International Symposium (Cat.No.95CH35844.), vol. pp. 1269, 1995.

[60] N.I. Vykhodtseva, K. Hynynen, and C. Damianou, Histologic effects of high intensity pulsed ultrasound exposure with subharmonic emission in rabbit brain in vivo *Ultrasound Med.Biol.*, vol. 21, pp. 969-979, 1995.

[61] W.F. Walker, Internal deformation of a uniform elastic solid by acoustic radiation force *J.Acoust.Soc.Am.*, vol. 105, pp. 2508-2518, 1999.

[62] T. Wu, J.P. Felmlee, S.J. Riederer, and R.L. Ehman, MR Elastography of Focused Ultrasound Induced Thermal Lesions, Proc. Intl. Conf. of Mag. Res. in Med., 1999.